Collaborative project*

Project acronym: SNM

Project full title: "**Single Nanometer Manufacturing for beyond CMOS devices**"

Grant agreement no: 318804

Deliverable: D4.5 ("Helium Ion Beam Lithography and Limits for SNL")

Name of the coordinating person: Prof. Dr. Ivo W. Rangelow, Email: ivo.rangelow@tu-ilmenau.de

List of participants:

Participant no.	Participant organisation name	Part. short name	Activity Type	Country
1 (Co)	Technische Universität Ilmenau	**TUIL**	HER	Germany
2	EV Group E. Thallner GmbH	**EVG**	IND; End-user	Austria
3	IMEC	**IMEC**	RES	Belgium
4	Mikrosistemi Ltd	**µS**	SME; End-User	Bulgaria
5	Universität Bayreuth	**UBT**	HER	Germany
6	Technische Universiteit Delft	**TUD**	HER	Netherlands
7	Spanish National Research Council	**CSIC**	RES	Spain
8	IBM Research GmbH	**IBM**	IND; End-user	Switzerland
9	École polytechnique fédérale de Lausanne	**EPFL**	HER	Switzerland
10	SwissLitho AG	**SL**	SME; End-User	Switzerland
11	Oxford Instruments Nanotechnology Tools Ltd	**OINT**	IND; End-user	UK
12	Imperial College London	**IMPERIAL**	HER	UK
13	The Open University	**OU**	HER	UK
14	Oxford Scientific Consultants Ltd	**OSC**	SME	UK
15	VSL Dutch Metrology Institute	**VSL**	IND	Netherlands
16	University of Liverpool	**ULIV**	HER	UK

SNM Work Package 4 Deliverable: D4.5 ("Helium Ion Beam Lithography and Limits for SNL")										
Lead beneficiary number	14	**Nature**	R	**Dissemination level**	PU					
Estimated Person-months	12									
Person-months by partner for the Deliverable	OSC									
	12									
Estimated Delivery Date	31/12/2016	**Delivery Date**	31/12/2016							
Author	• Lead Author: Philip D Prewett									
Reviewed by:	• WP4 Leader: Cornelis W Hagen • WPG1 Leader: Armin Knoll • Coordinator: Ivo W. Rangelow									
Criteria and Achieved Results	**Criteria**	**Achieved result**								
	Report detailed results of helium ion beam lithography experiments including novel work on proximity effect and optimised fullerene resists.	Achieved: see report below.								

Description of the Deliverable	• Report of experiments and modelling of helium ion beam lithography including discussions of how it compares with electron beam lithography and gallium focused ion beam lithography. Its differences from hydrogen ion beam stencil beam projection lithography (CHARPAN™) are considered. In particular, helium ion beam lithography is intended for flexible prototyping lithography rather than for mask making and high throughput. It also has higher resolution: <8nm compared with 20nm for CHARPAN™. Results of the use of helium ion beam lithography with a novel fullerene resist are included in the report together with experiments quantifying the low proximity effect.
Explanation of Differences between Estimation and Realisation	The report includes some work using gallium ion beam lithography. This was due in part to the need to maintain experiments during periods when the helium ion beam tool was out of commission and under repair but was also useful to compare and contrast the two lithographic techniques.
Metrology comments	The ORION™ helium ion beam tool used in the lithography experiments is essentially a helium ion microscope with an added pattern generator for lithography. As such, it was used alongside lithography in its other role as a scanning microscope and as the first line metrology tool for the OSC team with results as seen throughout the report. The ORION™ was also used in the metrology benchmarking experiments and for contributions to Metrology deliverable D7.6.

Contents

Foreword

This report includes contributions in collaboration with OSC from the Universities of Southampton and Birmingham. The Helium Ion Microscope facility at U Southampton was used for the Helium Ion Microscope (HIM) based experiments. The fullerene resist used in scanning helium ion beam lithography (SHIBL) experiments was developed in collaboration with Irresistible Materials Ltd.; OSC's PhD student Miss Sally Shi carried out the Helium Ion Beam Lithography and the associated Helium Ion Microscopy; Alex Robinson led the fullerene resist work. Other contributors to the HIM work were Ejaz Huq, Stuart Boden and Darren Bagnall. The gallium focused ion beam experiments were carried out in collaboration with Aydin Sabouri and Carl Anthony at Birmingham University's MicroEngineering and Nanotechnology Group and some key results are reported in Annexe II. The Annexes are an essential part of the report where detailed experimental results have been located to ensure the clarity and readability of the main body of the text.

Executive Summary

We report experiments and modelling of helium ion beam lithography including discussions of how it compares with electron beam lithography and gallium focused ion beam lithography. Its differences from hydrogen ion beam stencil beam projection lithography (CHARPAN™) are considered. In particular, helium ion beam lithography is intended for flexible prototyping lithography rather than for mask making and high throughput. It also has higher resolution: <8nm compared with 20nm for CHARPAN™. Results of the use of helium ion beam lithography with a novel fullerene resist are included in the report together with experiments quantifying the low proximity effect.

The sensitivity of the preferred formulation of fullerene resist in scanning ion beam lithography (SHIBL) was measured to be 50μC/cm^2 which is 500X greater than its sensitivity in electron beam lithography; its contrast in SHIBL is 2.8. The resolution limits of scanning helium ion beam lithography were explored, including establishment of the optimum linewidth CD (7.3nm) at which low values of line edge roughness were obtained (2.95 ±0.06nm, 3 sigma). High resolution sparse and dense lines in fullerene resist were achieved down to a resolvable limit of 6nm due to shot noise.

The annexes provide a table summarizing the experimental results, examples of computer modelling, results of gallium ion beam lithography and the text of a submitted paper describing the novel fullerene resists from WP5 (OSC and IM Ltd) used in the lithography experiments.

1. Introduction

Scanning Ion Beam Lithography is similar to electron beam lithography (EBL) as used for research and batch manufacturing. The first systems, developed in the 1980s [1, 2], used a Ga^+ liquid metal ion source (LMIS) [3, 4]. They had advantages over EBL because of the absence of proximity effect due to electron backscattering which limits the pattern density of high resolution features using EBL [5]. The heavy Ga^+ ions are free of proximity effect, but resist sputter erosion and low penetration depth, demanding ultra - thin pinhole free resist, together with heavy ion substrate damage limited the uptake of scanning ion beam lithography. This situation was revolutionized several decades later by the invention of the ultra - high brightness light ion He^+ Atomic Level Ion Source (ALIS) used by Carl Zeiss in their ORION™ Plus system [6]. This is similar to an EBL tool, being based on a scanning spot system derived from a high brightness charged particle source - in this case the ALIS He^+ source which has a brightness three orders of magnitude greater than the conventional liquid metal ion source. It is also free of the source halo which provides an additional quasi proximity effect when using the Ga^+ LMIS [7]. The ALIS source depends on the emission of He^+ from gas ionized at the trimer of atoms terminating an ultra-sharp tungsten tip, held at a temperature of -150°C. The operation of the ALIS is shown schematically in Fig 1 [6]. The lighter and less damaging He^+ ions enable the ORION™ to be used both as a scanning ion beam lithography systems and as a He Ion Microscope (HIM). The focusing and scanning of the He^+ beam in the ORION™ Plus is achieved using electric lenses and scan plates as shown schematically in Fig 2. This is because the greater electric "stiffness" of the ion beam compared to electrons prevents the use of magnetic focus and deflection coils. The scanner – blanking control is achieved using external hardware and software from Xenos. The scan field is 900µm x 900µm, but for high resolution patterning the field is limited to 10µm x 10µm to prevent beam distortion effects; there is no laser stage.

OSC's objectives in the SNM Project included an investigation of the use of the ORION™ system as a dual purpose lithography and microscope tool for patterning and measurement in the sub 10nm regime. The flexibility of the ORION™ as a multi-pattern vector spot scanning tool distinguishes it from an ion projection system like CHARPAN™ [8] which is designed to provide multiple exposures of the same pattern, projected using a sophisticated dedicated stencil, and which, unlike ORION™, cannot be used as an ion microscope. The CHARPAN™ tool has poorer resolution (20nm) using H+ ions compared with <8nm for ORION™ with its

ultimate Gaussian probe diameter of 0.4nm. Unlike CHARPAN™, the ORION™ HIM is not intended for production. Instead, with its sub 10nm resolution and dual purpose capability – combined nanowriter and microscope – it is more suited to rapid prototyping and batch fabrication applications. OSC's objectives within Task 4.15 (Work Package 4) of the SNM Project have been to explore the potential of scanning helium ion beam lithography (SHIBL) as an ultra-high resolution nanowriter for sparse and dense patterns. The task was linked to Task 5.4 in Work Package 5 where OSC was responsible for development, optimization and application of a novel fullerene molecular resist. In this way, the key objectives of exploring capabilities and limits of SHIBL for single nanometre lithography were investigated and tested.

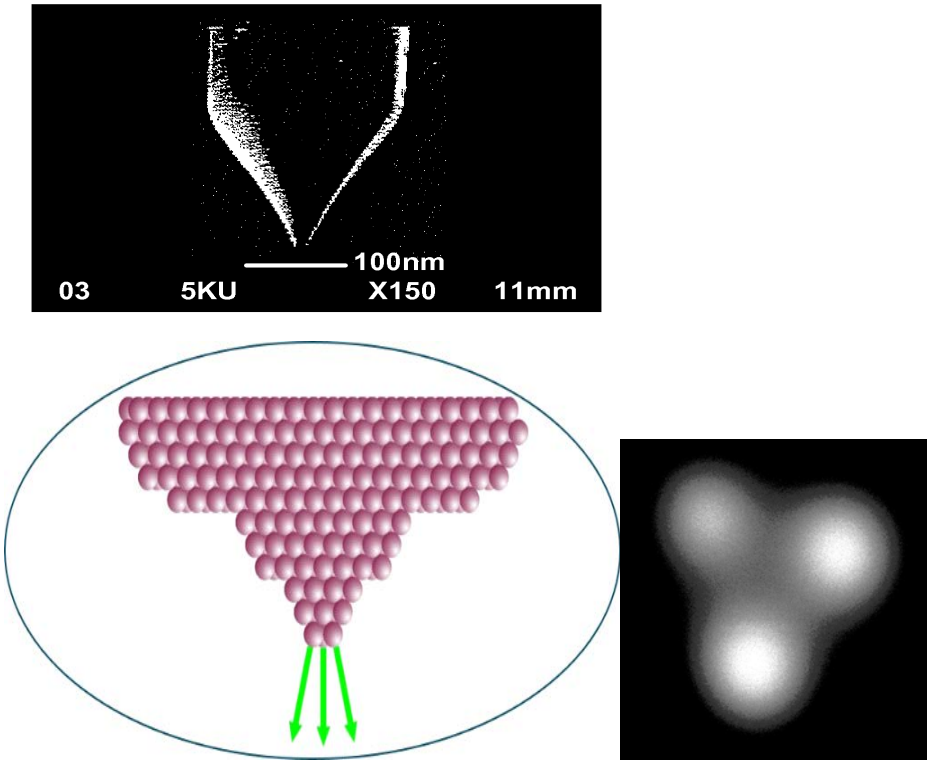

Fig 1 Trimer gas field ion source ALIS operating at <-150˜C [6]

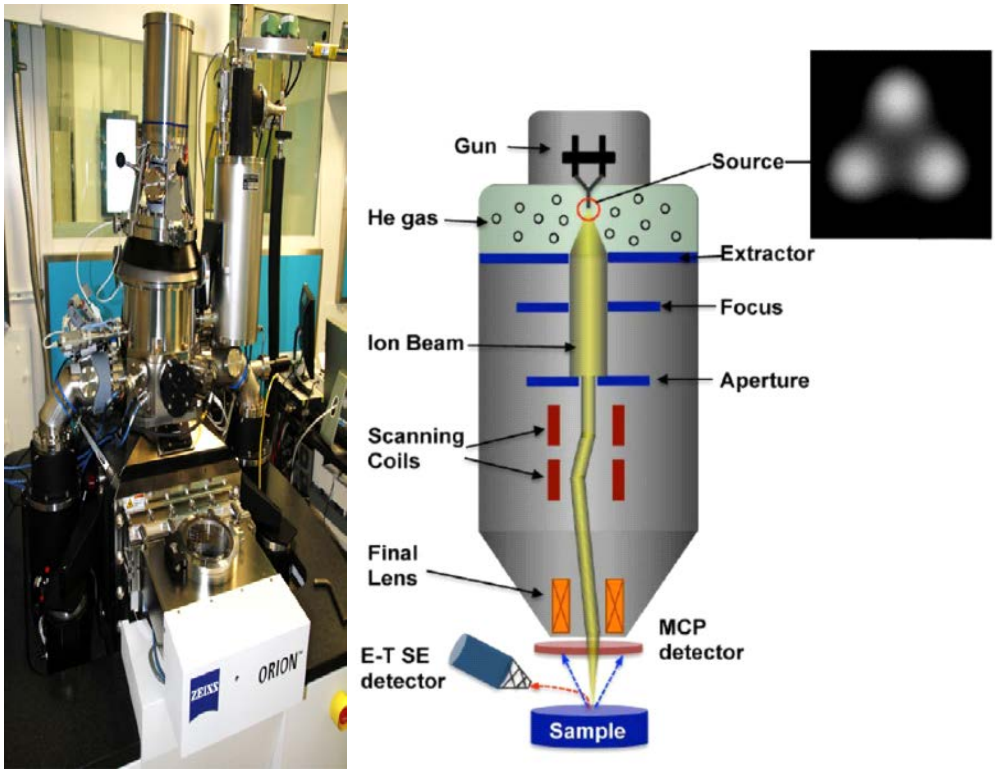

(a) (b)

Fig 2 (a) ORION™ Plus He Ion Microscope from Carl Zeiss GmbH (b) Schematic of He^+ ion focusing column showing electric focusing and scan electrodes

For ion optical focusing columns like that shown in Fig 2, the quantum mechanical wavelength determines the diffraction contribution to the ultimate probe size d_p for all forms of charged particle microscopy and lithography, according to the Root-Power-Sum (RPS) addition formula [9,10]:

$$d_p = \left\{ \left[\left(d_{df}^4 + d_s^4 \right)^{\frac{1.3}{4}} + d_g^{1.3} \right]^{\frac{2}{1.3}} + d_c^2 \right\}^{\frac{1}{2}} \qquad (1)$$

Where d_s, d_c and d_{df} are the contributions to spot size due to spherical aberration, chromatic aberration and quantum mechanical diffraction. The Gaussian optical image size magnified through the lens optics is d_g. Determining the probe size in the key chromatic aberration dominated regime, the energy spread of He^+ ions from the ALIS are in the range 0.25eV - 0.5eV FWHM [7] - an order of magnitude less than for Ga^+ ions from the LMIS [11]. The ultimate spot size of the ORION™ tool is 0.4nm, making it ideal for the SNM project domain.

2. SHIBL and its Advantages

After the ultimate probe size is established, the ability to perform lithography using charged particle beams and the resolution obtained are determined by the scattering of the beam in the resist layer and the underlying substrate. Scattering and range for different charged particles can be calculated using Monte Carlo simulation codes for ions (SRIM™ [12]) and electrons (CASINO [13]) with results as shown in Fig 3 [6, 12, 13].

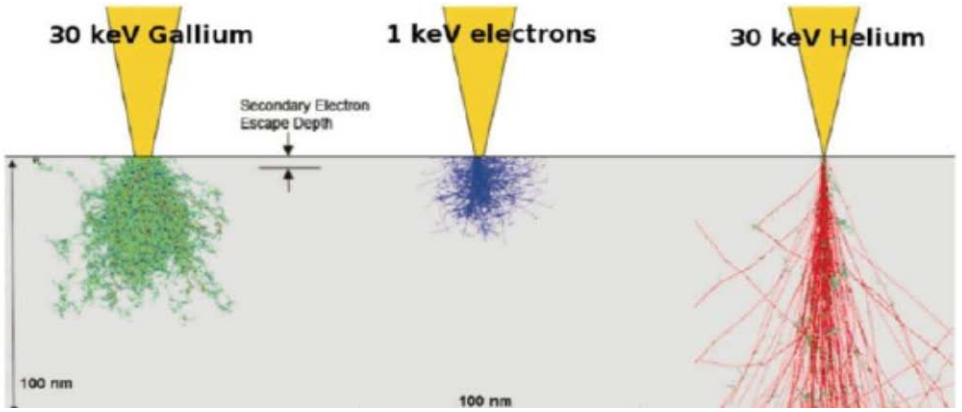

Fig 3 Modelling of charged particle penetration and scattering in silicon [6, 12,13]

The advantages of SHIBL using He^+ ions over SIBL using Ga^+ ions is clear from the reduced lateral spread of the beam in the top 10-20nm of the surface where the ultrathin resist layer is located in nanolithography. In practice, the effect of the resist can be ignored and the lateral spread is determined by the wafer substrate alone. The resist layer is exposed not by the primary ions but by the electrons they generate, which have lower energies compatible with forming the chemical bonds of the negative tone resist – the so-called "δ-rays".

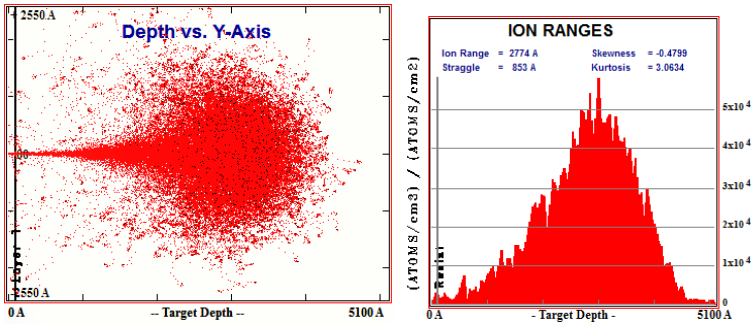

(a) (b)

Fig 4 (a) He^+ ion tracks through a 10nm thick resist on Si target (30keV) (b) Ion range. Calculated using SRIM™ [11].

We have calculated the ion tracks and the mean ion implantation range for He^+ ions in different materials using the SRIM™ code from Ziegler [12]. The resist-on-silicon system has been modelled using a 10nm layer of carbon on silicon wafer. This target is impacted with He^+ ions at the optimum energy of 30keV. The results, plotted in Fig 4, show the He^+ ions implanted deep in the silicon with a mean projected range and straggle calculated as R_p= 277nm±43nm. It is important to note that there is minimal backscattering of ions at 0.13% of the incident beam, which indicates that proximity effect will be negligible – a prediction confirmed by experiment below. The modelling shows a strong dependence on both target ion and substrate as seen in Table 1.

Ion	Range & Straggle in Si or Au
$^{1}H^{+}$	301±28nm 137±28nm
$^{4}He^{+}$	277±43nm 89±21nm
$^{69,71}Ga^{+}$	26±4nm 14±3nm

Table 1: Calculated range data for 30keV ions in 10nm resist on Si and Au (4000 ions)

In the case of the light ions H^+ and He^+ there is no surface erosion according to SRIM™ modelling so that the implanted ion distribution may be approximated by a Gaussian distribution centred on the mean projected range R (see Annexe II):

$$n(x) = \frac{D}{\sigma\sqrt{2\pi}} e^{-\frac{(x-R)^2}{2\sigma^2}} \qquad (2)$$

Where $n(x)$ cm^{-3} is the number density of ions at depth x, D cm^{-2} is the ion dose and σ is the standard deviation or straggle. Where there is sputter erosion of the resist layer as in the case of Ga^+ ions, the implanted ion distribution is a sum of Gaussians – an error function as shown in Annexe II – with its maximum value at the eroded surface which may be approximated to

$$\frac{n(x)}{(\rho/\gamma M)} = \frac{erf\frac{R-x}{\sigma\sqrt{2}} + erf\frac{x+X-R}{\sigma\sqrt{2}}}{1+erf\frac{R}{\sigma\sqrt{2}}} \qquad (3)$$

Where X is thickness of the resist eroded by sputtering, ρ, γ are the substrate density and sputter yield measured in atoms/ion under He^+ bombardment at 30 keV ion energy; M is the mass of the target atoms (See Annexe II for further discussion of this equation).

The very short range of Ga^+ ions is a *prima facie* advantage in that more of the beam energy is deposited close to the surface but this is offset by the greater sputter yield of the heavy Ga^+ ions which remove resist and damage the substrate. Of particular importance for proximity effect is the fraction of incident ions which are backscattered into the resist from the substrate. In the case of He^+ with a resist on Si substrate at 30keVbeam energy this is 0.13% rising to 0.3% for H^+ under the same conditions. These values are insignificant in the context of proximity effect. The 10nm resist on Si wafer system used in SHIBL is more than an order of magnitude thinner than the mean projected range and plays little or no part in energy deposition from the primary beam: the resist is exposed by secondary electrons from the substrate.

Implanted He^+ ions are found to produce pockets of He gas below the target surface which can, at high ion doses, create bubbles which distort the surface topography through the formation of nanoscale domes. In contrast, the widely used Ga^+ ions can form liquid precipitates with associated hydrodynamic effects. These were the subject of benchmark studies in the frame of SNM with results as summarized more fully in Annexe II below.

3. Experiments

3.1 Baseline tests with PMMA

The positive tone resist polymethylmethacrylate (PMMA) has played a key role in the development of both EBL and ion beam lithography. It was therefore the positive tone resist of choice and was used in baseline experiments in the project, including both sensitivity measurements and proximity effect evaluations for SHIBL.

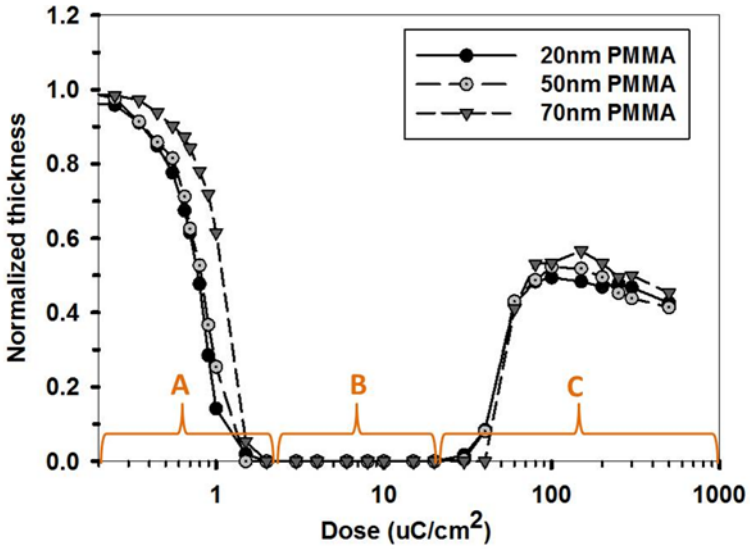

Fig 5 Sensitivity results using SHIBL to expose PMMA resist (30keV ions)

The thickness remaining after development was measured as a function of ion dose for three spun thicknesses of PMMA – 20nm, 50nm and 70nm – with the results plotted in Fig 5. The ion dose required to clear the positive tone PMMA (region A) is ~2μC/cm^2 which is more than three orders of magnitude lower than that for EBL. At doses in the range 2 - 30μC/cm^2 the ion beam dose continues to clear the resist which is in a transitional response state (region B). At higher doses the PMMA changes from positive to negative tone (region C). Unfortunately, despite its high sensitivity and tone flexibility under 30keV He^+ ion irradiation, PMMA has poor durability in plasma etch, making it unsuitable for the pattern transfer processes in SNM. For this reason, apart from early baseline experiments, we have focused attention on the novel fullerene resists developed with Irresistible Materials Ltd, as reported in section 3.4 below.

The results in Fig 5 show that, within the limits of experimental error, the sensitivity of PMMA in SHIBL is independent of resist thickness for values of 20nm, 50nm and 70nm. This is consistent with the ion mean range data in Fig 3 and Fig 4: the ion energy is deposited below the resist layer for values in this range so that the dependence of sensitivity on resist thickness is weak as seen in Fig 5.

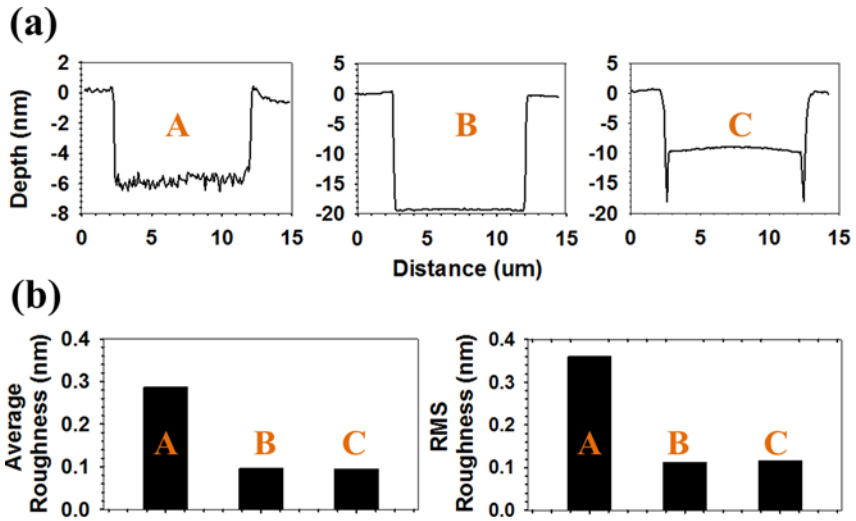

Fig 6 Roughness measurements of patterns exposed using SHIBL in PMMA

AFM measurements of surface roughness were carried out for SHIBL - exposed PMMA in all three regions with the results shown in Fig 6 for doses ~0.6μC cm^{-2}, ~ 2- 30μC cm^{-2} and ≥20μC cm^{-2} in regions A, B and C respectively. The average value of surface roughness is below 0.3nm in region A , close to the helium ion beam diameter, falling to identical values below 0.1nm in region B (bare silicon surface) and region C (exposed PMMA in negative tone regime). The roughness value 0.1nm is the limit due to the polished wafer surface. These results show clearly the low effect on surface roughness of the SHIBL process as indicated from the modelling work in Figs 3 and 4 which predicted zero sputtering at 30keV. The conclusion from the results for region A is that the surface roughness is either due to a very small sputtering effect, not predicted by the simulations, or to shot noise.

Notwithstanding the poor plasma etch durability of PMMA, its high sensitivity in SHIBL demonstrates good baseline performance for fast prototyping of structures and devices. We shall show below the use of SHIBL for a high sensitivity novel fullerene resist with far better etch durability than PMMA (Section 3.3 *et. seq.*).

3.2 Proximity Effect in SHIBL

An investigation of the Proximity Effect for SHIBL has been carried out using the positive tone resist poly methyl methacrylate or PMMA $(C_5O_2H_8)_n$ as part of the SNM Project. This is an appropriate choice of resist given the large number of studies reported in the literature for EBL

proximity effects in PMMA since the earliest work of Phang [5]. Fig 7 shows the results of our SHIBL experiments on Proximity Effect in PMMA following Stevens et al [14] who investigated the effect for electron beam lithography. The method uses 2D donut (annulus) shaped ring exposures in positive tone PMMA, revealing the variation of pattern with dose. The outer radius of the ring was fixed at 200nm while the inner radius R_1 was varied in the range 5nm to 125nm. The dose was varied in the range $0.3 - 200 \mu C / cm^2$; the SHIBL beam conditions were 30keV He^+ energy with an ion current of 0.3pA. The PMMA was spun to a thickness of 20nm and prebaked for 70s at 180°C; development was carried out in MIBK/IPA (1:3) for 60s.

The principal effect of the proximity dose is to reduce the diameter of the central remaining core of resist with increase of dose as seen from the matrix of patterns in Fig 7. The experiment relies upon identification of the value of the set inner radius of the donut for which the resist is totally cleared right to the centre P and the donut annulus becomes a full circle. In the SEM image of Fig 7, as the applied dose increases downwards by row from the top, the value of R_1 for total clear out of PMMA shifts by column to the left. The radial symmetry of the donut makes mathematical modelling relatively simple using a double Gaussian approximation to model the beam transfer function in the resist [14, 15].

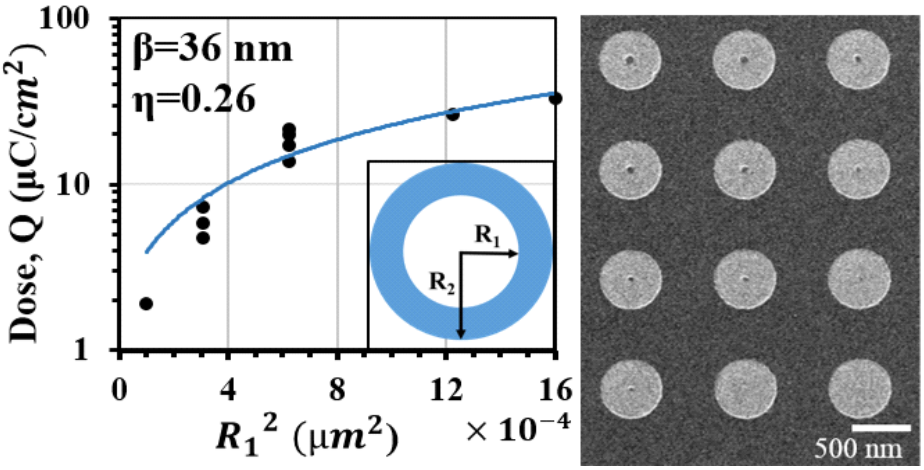

Fig 7 Variation with dose of donut inner radius for which the exposed pattern in PMMA becomes a full circle due to proximity effect in He^+ SHIBL at 30keV beam energy. The image shows the resist remaining (dark) after exposure and development. R_1 increases by column from right to left; applied dose increases by row from top to bottom [15].

The double Gaussian at distance r from the centre P takes the form

$$f(r) = \frac{1}{\pi(1+\eta)}\left[\frac{1}{\alpha^2}e^{-(\frac{r}{\alpha})^2} + \frac{\eta}{\beta^2}e^{-(\frac{r}{\beta})^2}\right] \qquad (4)$$

Where α is the standard deviation of the forward scattered ions distribution and β is the standard deviation of the backscattered ion distribution; β is the ratio of energies deposited in the resist by forward and backscattered ions. The total dose received by the patterned cell for an applied dose Q is

$$D(R_1) = 2\pi Q \int_{R1}^{\infty} f(r)dr = \frac{Q}{1+\eta}\left[e^{-(\frac{R1}{\alpha})^2} + \eta e^{-(\frac{R_1}{\beta})^2} \right] \qquad (5)$$

Where the approximation $R_2 \to \infty$ has been applied. A further approximation is possible, since $R_1 >> \alpha$ (justified by the SRIM™ modelling in Fig 4) so that equation 5 may be simplified to

$$D(R_1) = \frac{Q}{1+\eta}\eta e^{-(\frac{R_1}{\beta})^2} \qquad (6)$$

From which $$\ln Q = \left(\frac{R_1}{\beta}\right)^2 + \ln\left[\frac{D(1+\eta)}{\eta}\right] \qquad (7)$$

The simplified equation has been fitted to the experimental results as shown in Fig 7. This gives a forward energy deposition efficiency of η=26% and a standard deviation of β=36nm for the backscattered energy spatial distribution which is almost two orders of magnitude smaller than comparable EBL values. The conclusion is that, while there is some residual proximity effect in the case of SHIBL because of the lightness of the He^+ ions, these effects are negligible when compared to those due to electron backscattering in EBL.

It is clear from the SRIM™ modelling results that back scattering of He^+ ions from the resist-on-silicon target is too low (0.13% of incident ions) to be responsible for the small proximity effect in SHIBL. Instead, this is almost certainly due to ion induced secondary electrons.

3.3 SHIBL with Novel Fullerene Resist

Irresistible Materials Ltd and Birmingham University UK provided novel fullerene resists for the SNM project's SHIBL resolution limit experiments which were optimized for SHIBL as part of SNM [see Annexe III]. These resists are polymerized from the C_{60} molecule, selected for its sub nanometre dimensions (0.7nm) and its stability. Before the EU SNM project, the state of the art in SHIBL was represented by the work of Sidorkin *et al* at TU Delft [16] who demonstrated sub 10nm linewidth lithography in hydrogen silsesquioxane (HSQ) electron beam resist using He^+ ions. Following this, the SNM project has explored the use of a number

of the novel fullerene resists chosen for their superior performance in plasma etch pattern transfer applications. These resists have demonstrated exceptional plasma etch resistance and stability together with resolution approaching 7nm in SHIBL [17]. The state of the art in Fullerene resist technology, their chemistry and the advantages of their latest forms, such as spin coatability to give ultra - thin pinhole free layers, are reviewed in the SNM Technology Book and reproduced in Annexe III [18, 19, 20]. The IM fullerene resist provides a high sensitivity resist in two forms: HM-01C cast in chlorobenzene solvent and HM-01A cast in anisole. Both formulations are developed using cyclohexanone.

3.3.1 Resist Sensitivity in SHIBL

Following a pre-exposure bake on a hotplate at 70 °C for 5 minutes, the samples were exposed in a HIM (ORION^{TM} Plus, Carl Zeiss) to a 30keV focused helium ion beam at a working distance of 7 mm. Helium pressure was maintained at 5×10^{-6} Torr during the exposure and a 10µm beam limiting aperture was selected. A beam current of 5pA was used to expose 10µm x 10µm areas efficiently in the resist sensitivity evaluation, using a single-pass centre to edge writing strategy. (For the high resolution patterning experiments, a small beam current of 0.5pA was applied to achieve optimal beam spot size for single-pass, single pixel line scans).The exposed samples were developed in cyclohexanone for 20 seconds and rinsed in isopropyl alcohol (IPA) for 10 seconds to produce various negative tone patterns, then blow-dried in nitrogen. For a direct comparison of resist sensitivities in SHIBL and EBL, the HM-01 samples were also exposed in the Gemini FEG-SEM (NVision 40 FIB SEM with pattern generator from Raith GmbH) to a 30keV focused electron beam generated from a Schottky source at a working distance of 10mm. A current of 5.8nA was used during the e-beam exposure with a beam limiting aperture of 120µm. The sample preparation and the subsequent development process were identical in both SHIBL and EBL processes. Patterned samples were characterised using both atomic force microscopy (AFM: Multimode^{TM}, Veeco Inc) and HIM. An array of 5µm × 10µm areas were exposed with SHIBL for doses ranging from 0 to 288µC/cm^2. The residual film thickness after development was measured using AFM. Figure 8(a) shows an optical micrograph and Fig 8(b) shows an AFM image of five of the exposed areas. The first dose area appears shallower with a lower contrast compared to the other four. The line profile obtained from the AFM (Figure 8 (c)) confirms a thinner resist remaining for the first area due to underexposure, whilst thicker resist layers remain for other areas that were fully exposed. The dose response curve for HM-01A was determined (see Figure 8(d)) by plotting the normalized resist thickness

against the logarithm of dose, showing that HM-01A exhibits negative tone behaviour in SHIBL with a sensitivity (50% of final full exposed thickness) of ~40μC/cm^2. An identical procedure was followed on the HM-01A sample exposed in EBL at 30keV and the dose response curve is also plotted in Figure 8(d) for comparison. In EBL, the sensitivity of the HM-01A fullerene derivative resist is 20000μC/cm^2. Hence, there is a 500 times improvement in sensitivity using SHIBL to expose this resist. This results in a significantly reduced required exposure time for a given beam current, with consequently improved throughput efficiency. The areal dose used in SHIBL corresponds to an ion density of 2.5 × 10^{14} ions/cm^2, which is sufficiently low to limit physical damage by ion implantation to the underlying substrate in these regions. This means that SHIBL causes little sub-surface modification, such as bubble formation and swelling, which can limit the highest achievable resolution and prevent subsequent pattern transfer (see Annexe II and SNM deliverable D7.6 for further discussion of the He bubble phenomenon).

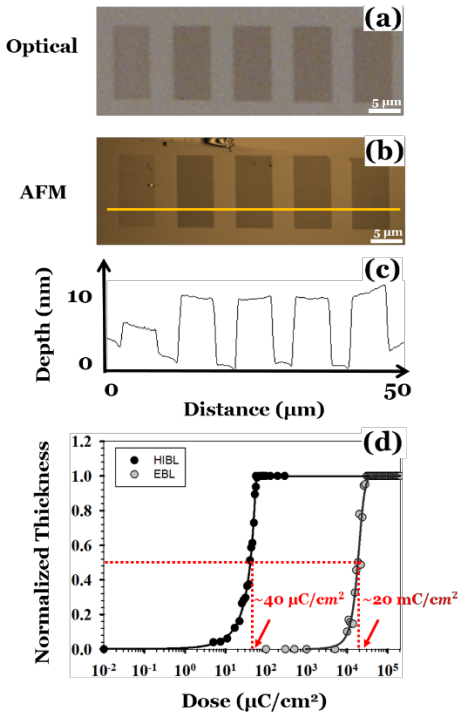

Figure 8. (a) Optical micrograph, (b) AFM image and (c) Line profile (values plotted were averaged from a 20-pixel range) of the same dose test areas on the ~10 nm fullerene derivative resist (HM-01A) after development. The applied doses are 37.9, 56.5, 85.0, 128.0 and 192.0μC/cm^2 from left to right; (d) Comparison of the dose response curves for HM-01 in SHIBL and EBL. The sensitivities are measured to be 40 μC/cm^2 and 20 mC/cm^2, respectively, revealing 500 times sensitivity improvement in SHIBL [17]

As already mentioned, HM-01 novel fullerene resist is soluble in both chlorobenzene and

anisole solvents. The HM-01A formulation is preferred for environmental and safety reasons. A further set of experiments to compare contrast values for HM-01A and HM-01C gave the results shown in Fig 9. The sensitivity values from these results are 50μC/cm^2 for HM-01A and 30μC/cm^2 for HM-01C. There is thus a benefit in terms of speed to using the chlorobenzene casting solvent. The contrast values of the chlorobenzene and anisole version measured from Fig 9 are, within the limits of experimental error, the same at Υ = 2.8 and 2.9.

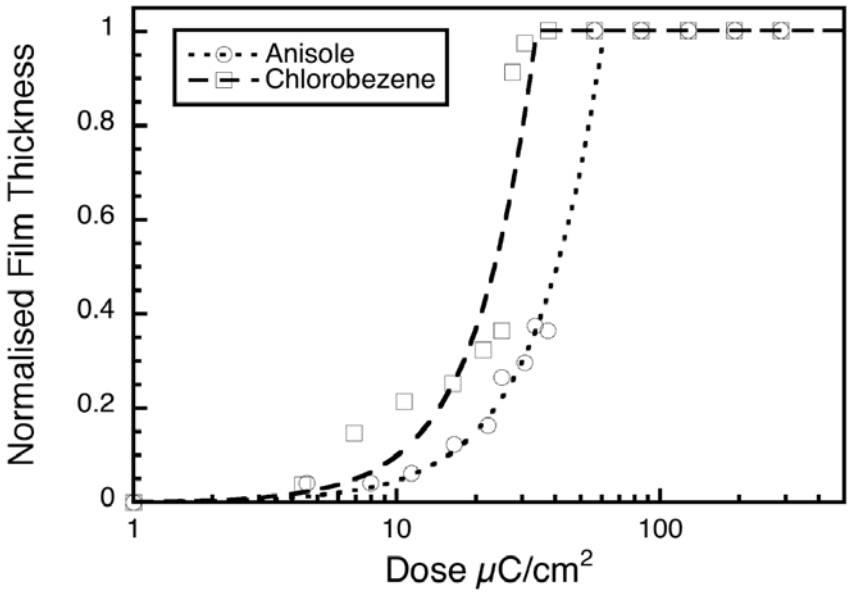

Fig 9 Exposure – dose curves for fullerene resists HM-01C and HM-01A in SHIBL

The HM-01 formulation has been tested in comparison with a number of novel resists within SNM for etch durability with outstanding performance being recorded [21].

3.4 High Resolution Lithography Using SHIBL

We will focus here on the preferred version HM-01A. This a spin - coatable liquid resist giving a thickness of 10nm when spun at a speed of 4,000 rpm on a silicon substrate. In the absence of an ellipsometer model for the novel C_{60} resist, layer thickness was measured by removing the resist layer using adhesive tape, then measuring its thickness with a surface profilometer. As discussed in Annexe III, it is necessary for high resolution lithography in the sub 10nm regime to employ resist layers of 10nm or less in order to avoid pattern collapse (critical aspect ratio for collapse – CARC) [22].

3.4.1 *High Resolution Sparse Feature Patterning*

Following a Post Application Bake at 70°C for 5min, lithography of isolated lines was carried out to measure the ultimate resolution of the SHIBL method for fullerene resist with the results

shown in the He Ion Microscope (HIM) image shown below (Fig 10).

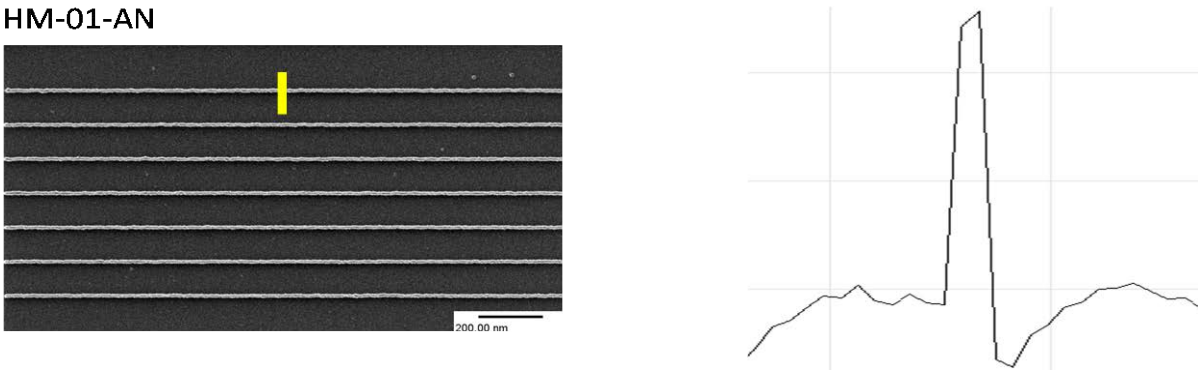

Fig 10 Isolated Lines 8nm wide in HM-01A resist with optimized exposure line dose of 0.08nC/cm – He Ion Microscope image. A scan of contrast variation across the line is shown at right.

The lines were written at an optimized dose of 0.08nC/cm. Full write data conditions were:

Beam Energy: 30keV

Beam Current: 0.5pA

Beam diameter: ~0.35-0.5nm

Line write speed: 1nm/16µs

Resist spin speed: 4000rpm

Resist thickness: 10nm

Post application bake temperature and time: 70°C for 5min

Developer: cyclohexanone for 20 s followed by IPA (10s)

The metrology function of the ORION™ tool was applied to the HIM image to measure linewidth as shown in Fig 10. The imaging conditions were:

Imaging Data:

Beam Energy: 30keV

Beam current: 0.5pA

Beam diameter: ~0.35nm - 0.5nm

Lines per frame: 128

The linewidth of these sparse lines is 8nm as measured from Fig 10.

An exposure dose optimization matrix for SHIBL using HM-01A resist showing line width CD and lithographic quality as a function of ion dose is shown in Fig 11, again imaged using the

ORION™ tool in HIM mode. The optimum linewidth CD and ion dose in these experiments were 7.2nm and 0.075nC/cm respectively.

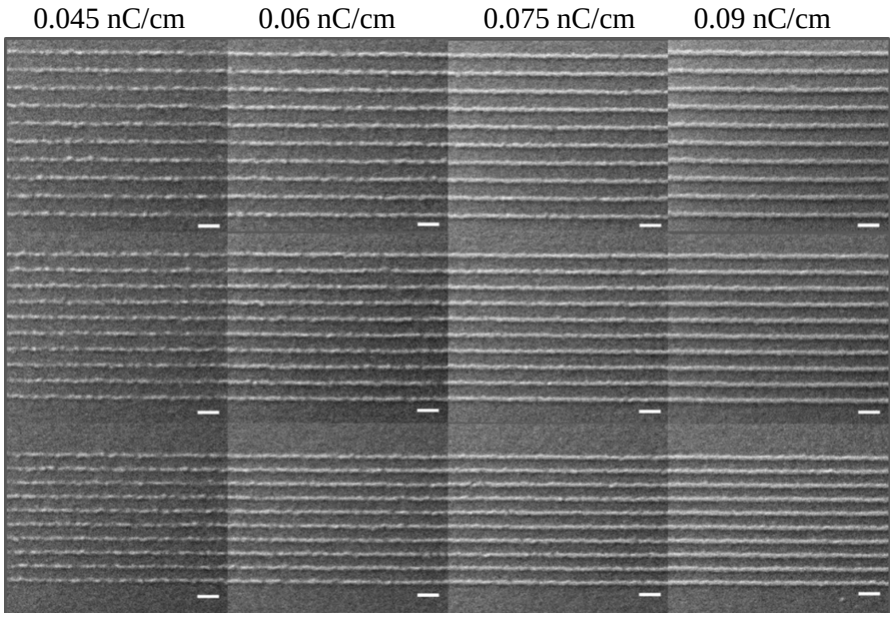

Fig 11 High resolution exposure dose matrix: SHIBL in HM-01A fullerene resist

A series of experiments was carried out to determine the limits of SHIBL using the fullerene resist for sparse and dense patterns as a function of line dose. Measurements of linewidth CD (LW) and line edge roughness (LER) were made using the ORION™ Plus in scanning ion microscope mode (see also WP7 and deliverable D7.6).To find the minimum limit of LW achievable, arrays of 1.5µm long single pixel sparsely spaced lines were exposed with line doses ranging from 0.005 to 0.1nC/cm. Fig 12 shows HIM images of sparsely spaced lines at 40nm pitch on 10nm thick HM-01 resist after the development process. The lines are well defined with high contrast to the substrate. The LWs were measured using He ion induced secondary electron contrast (ISE) with 20 pixel line averaging; the average value was taken as the CD. The CD varies from 7.3nm to 8.3nm depending on dose. There is discontinuity in lines exposed at doses of 0.045nC/cm and 0.06nC/cm due to under - exposure.

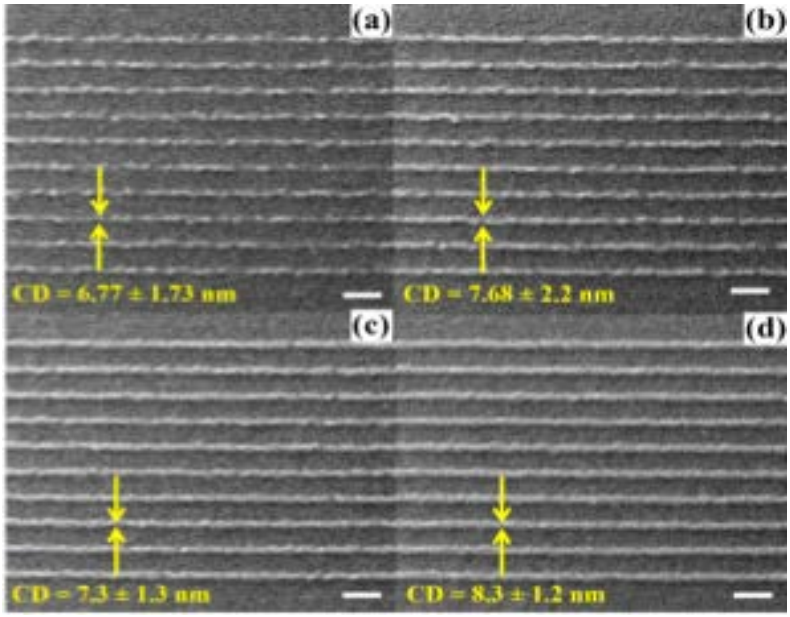

Fig 12 HIM images showing single pixel sparse line patterns exposed in 10nm thick HM-01 fullerene resist. Line doses: (a) 0.045nC/cm (b) 0.06nC/cm (c) 0.075nC/cm (d) 0.09nC/cm. Scale bar: 50nm

Some parts of the lines (Fig 12(b) and (d)) are significantly wider at approximately 9nm which is close to the nominal 10nm thickness of the resist. It is reasonable to conclude that very thin lines were fabricated but that some of these collapsed onto the substrate during development due to their high aspect ratio [22]. This results in a higher LW-CD compared with the optimum dose. Lines exposed at 0.09nC/cm are thicker due to over exposure. The optimum line dose was identified as 0.075nC/cm, at which the smallest CD was achieved. The line edge roughness (LER) values of the sparse lines as a function of line dose were extracted from the HIM images using the SuMMIT™ software package (EUV Corp), as seen from Table 2. The results are heavily dependent on the image processing methods but give a clear indication of trend. The greater values of LER in the underexposed patterns are due to discontinuities in the lines. This effect weakens as the dose is increased, producing lower LER values.

Dose nC/cm	0.045	0.06	0.075	0.09
LW-CD nm	6.77±1.73	7.68±2.2	7.3±1.3	8.3±1.2
LER nm	4.82±0.22	3.66±0.12	2.95±0.06	2.65±0.08

Table 2. Dose optimization results for sparse sub-10nm lines written by SHIBL in HM-01 fullerene resist showing variation of linewidth (LW) and line edge roughness (LER), 3 sigma range.

3.4.2. High resolution dense feature patterning

Experiments on dense feature patterning were carried out to determine the limits of pattern density for single pixel lines in HM-01 resist with pitches from 30nm down to 10nm and doses ranging from 0.005 to 0.1nC/cm. The results were, as usual, inspected using the ORION™ Plus in microscope mode. Fig 13(a)-(c) show the effect of decreasing pitch at a fixed dose of 0.075nC/cm for pitches of 20, 22 and 14.5nm respectively. The linewidths are effectively independent of pitch with a value close to 7.3nm in each case. These results confirm that the proximity effect may be ignored for SHIBL in the fullerene on silicon system. Fig 13(d)-(e) show the effect of increasing line dose at a fixed pitch of 145nm; the three doses are 0.045, 0.075 and 0.09nC/cm. The resulting LW-CDs are 6.8, 7.3 and 8.3nm respectively. These are, within the limits of experimental error, identical to the sparse line features for the same doses.

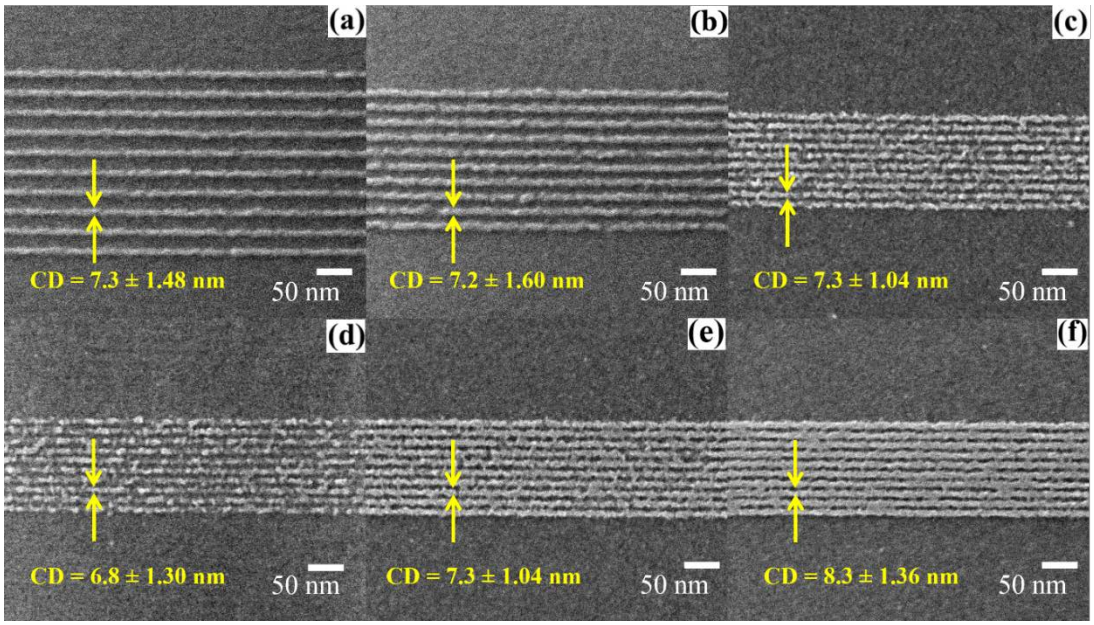

Fig 13 (a) - (c) HIM images showing the effect of decreasing pitch at a fixed line dose of 0.075nC/cm. Pitch values are (a) 30nm (b) 22nm (c) 145nm (d) - (f) Effects due to increasing dose at fixed pitch of 145nm. Doses: (d) 0.045nC/cm (e) 0.075nC/cm (f) 0.09nC/cm

The results for high density features are further confirmation of the insignificance of proximity effect using SHIBL with fullerene resist. The best high density results to date are continuous and well-defined lines with a pitch of 17nm and a 0.5 line/space ratio corresponding to a linewidth of 8.5nm as shown in the HIM image and associated contrast line profile in Fig 14. This is comparable to the capability of state of the art EBL tools despite the ORION™ Plus being a genuine dual purpose microscope and lithography tool which is not optimized for the tasks reported here and notwithstanding the use of an experimental resist.

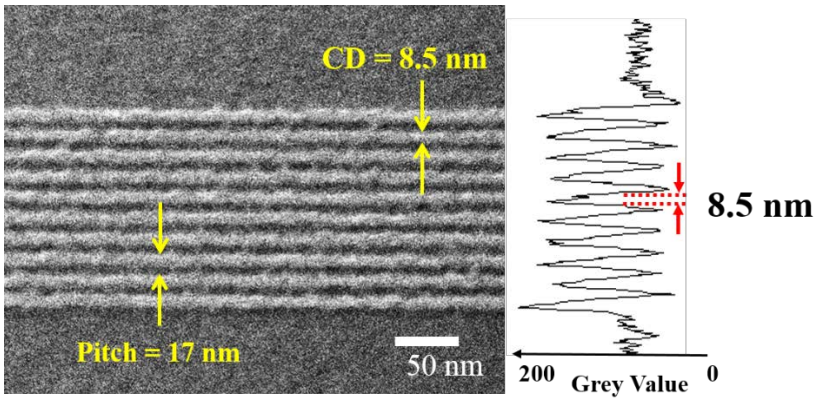

Fig 14. HIM image of dense single pixel lines exposed at 0.09nC/cm dose in 10nm thick HM-01A fullerene resist. The contrast profile reveals a pitch of 17nm and a linewidth of 8.5nm. The lines are well defined and continuous.

Fig 15 shows discontinuous but resolvable dense lines with a pitch of 12nm and a line/space ratio of 0.5, corresponding to a linewidth of just 6nm. These extremely narrow lines suffer from shot noise effects which results in random spatial fluctuations due to statistical variations in the number of ions per pixel absorbed by the resist [23]. The shot noise effect represents a fundamental limit of all charged particle lithography and affects both LW-CD and LER. It is more serious for high sensitivity resist when the number of charged particles per pixel is lower giving rise to a greater fractional fluctuation in dose per pixel.

In Fig 15 the line dose of 0.04nC/cm is equivalent to a He^+ dose of 25 ions/nm which produces a shot noise of 5:1, resulting in line discontinuity due to missing pixels. Fig 13(d)-(f) show how increased dose reduces shot noise and improves line continuity. Shot noise effects may also be mitigated by reducing pixel to pixel spacing or by partial overlap of adjacent pixels.

Finally, a further comment should be made concerning aspect ratio. As the features in Fig 13 approach an aspect ratio of 2:1 the likelihood of pattern collapse on development increases [21]. Hence for the smallest pitches - below 18nm - use of an even thinner resist film should ideally be employed.

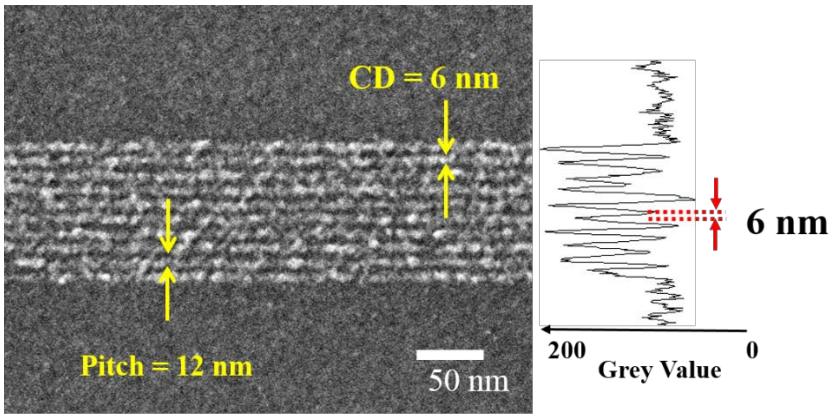

Fig 15. HIM image of dense single pixel lines exposed at 0.04nC/cm dose in 10um thick HM-01 fullerene resist. The contrast profile reveals a pitch of 12nm and a linewidth of 6nm. Shot noise effects are in evidence through missing pixels.

Conclusions

Scanning He^+ ion beam lithography (SHIBL) and helium ion microscopy (HIM) have been used to explore the limits of scanning helium ion beam lithography for nanoscale lithography in conjunction with a novel molecular (fullerene) resist HM-01 with two different casting solvents. This was developed further and customised for SHIBL with ultimate patterning capability down to 6 - 7nm. The He^+ sensitivity of HM-01 resist was shown to be 500X that of EBL. The limits of SHIBL were evaluated for 6nm patterns in HM-01A when shot noise gave rise to roughness due to missing pixels. Classical proximity effect evaluation experiments were conducted which verified the effective absence of proximity effects in SHIBL and this was further established for the novel fullerene resist. The potential of SHIBL and helium ion microscopy for high resolution nanolithography as an alternative to EBL was explored to its limits with a significant advance in the state of the art. A summary of the main results of the study in table form is provided at Annexe I.

References

[1] J R A Cleaver, P J Heard and H Ahmed (1983) SPIE **393**

[2] P J Heard (1985) PhD Thesis, Cambridge University, UK

[3] R Clampitt and D K Jefferies (1978) Nucl Instrum Meth **149**, 739

[4] P D Prewett and D K Jefferies (1980) J Phys D **13**, 1747

[5] J C Phang (1979) PhD Thesis, Cambridge University, UK

[6] R Hill, J Notte and B Ward (2008) Physics Procedia **1**, 135-141

[7] J W Ward, M W Utlaut, and R L Kubena (1987) J VacSciTechnol **B5**, 169 – 174

[8] F van Delft, R van der Laar, M Verschuuren, E Platzgummer and H Loeschner (2010) Microelectronic Eng **87**, 1062-1065

[9] J E Barth and P Kruit (1996) Optik (Jena) **101**, 101

[10] M S Bronsgeest, J E Barth, L W Swanson and P Kruit (2008) J Vac Sci Technol **B26**, 949

[11] J C Beckman, T H P Chang, A Wagner and R F W Pease (1997) J VacSciTechnol **B15**, 2332 -2336

[12] J F Ziegler, J P Biersack and U Littmark (1985) "The Stopping Range of Ions in Matter", Pergamon

[13] H Demers, N Poirier-Demers, AR Couture, D Joly, M Guilmane, N de Jonge and D Drouin (2011) Scanning **33**, 135-146

[14] L Stevens, R Jonkheere, E Froyen, S Decoutere and D Laneer (1986) MicroelectronEng **5**, 141-150

[15] X Shi, P D Prewett, E Huq, D M Bagnall and S A Boden (2015) Proc 41st In Conf Micro and Nano Engineering, The Hague, Netherlands, Sept 2015

[16]] V Sidorkin, E van Veldhoven, E van der Drift, P Alkemade, H Salemnik and D Maas (2009) J Vac Sci Technol**B27**, L18

[17] X Shi, P D Prewett, S E Huq, D M Bagnall, A P G Robinson and S A Boden (2016) Microelectron Eng **155**, 74-78

[18] T Tada and T Kanayama (1996) Jap J Appl Phys **35**, 1A

[19] F P Gibbons, A P G Robinson, R E Palmer, S Diegoli, M Manickam and J A Preece (2008) Adv Funct Mater **18**, 1977

[20] X Shi, D X Yang, S E Huq, S A Boden, D M Bagnall, R E Palmer, A P G Robinson and P D Prewett (2016) submitted for publication.

[21] JF de Marneffe, M Cooke, A Goodyear, NS Braithwaite, Y Sutton, M Bowden, E Altamirano-Sanchez, A Zotovich,, Z Otell, BT Chan, A Knoll, C Rawlings, U Duerig, M Spieser M Kaestner, C Neuber, I Rangelow. (2016) Advanced Etching for Nanodevices and 2D materials. *Presented at MNE 2016* SNM-1-52016. Accessible from: https://www.researchgate.net/publication/308764935_Advanced_Etching_for_Nano-devices_and_2D_materials.(IM-HM-01A resist is presented under the name MFHM1 in this work)

[22] D K Yoshimoto, C Higgins, A Raghunatha, J G Hartley, D L Goldfarb, H Kato, K Petrillo, M E Colburn, J Schefske, O Wood, T I Wallow (2011) Proc SPIE **7972**, 7920K.

[23] P Kruit and S W H Steenbrink (2006) Scanning **28**, 20-26

[24] P D Prewett and G L R Mair (1991) Focused Ion Beams from Liquid Metal Ion Sources, Research Studies Press, John Wiley and Sons Inc.

[25] F A Trumbore (1960) Bell System Technical Journal **39**:1, 205-233

[26] A Sabouri (2016), PhD Thesis, University of Birmingham, UK

[27] J. Naik, P. Prewett, K. Das, and A. Raychaudhuri, "Instabilities in Focused Ion Beam-patterned Au nanowires," *Microelectronic Engineering*, vol. 88, no. 9, pp. 2840-2843, 2011.

[28] A Bid, A Bora, and A. K. Raychaudhuri (2005) Phys Rev **B72**, 113415

[29] J J Kaufman, G Tao, S Shabahang, E H Banaei, D S Deng, X Liang, S G Johnson, Y Fink, and A F Abouraddy, "Structured spheres generated by an in-fibre fluid instability," *Nature*, vol. 487, no. 7408, pp. 463-467, 2012.

Annexe I: SHIBL – Summary of Experimental Results

Parameter			Value	Comments
Ion energy			30keV	Range 10 - 30keV
Beam diameter			0.3 - 0.5nm	
Beam current			5pA	
Ion mean range at 30keV		Carbon	272nm	
by target		Silicon	191nm	
		Gold	91nm	
Resist sensitivity PMMA		Pos	2μC/cm^2	at 30keV beam energy
		Neg	30μC/cm^2	
		Transition	2 - 30μC/cm^2	
Surface roughness			0.1 - 0.3nm	PMMA on silicon wafer
Proximity effect parameters			η=26%	Forward energy deposition
			β=36nm	Standard deviation
Resist contrast HM-01		Neg	2.6	
Resist sensitivity HM-01		Neg	40μC/cm^2	Novel fullerene
High resolution	optimal		7nm	
	limit		6nm	Shot noise limit
Optimum dose (linescan)			0.075C/cm	
Write speed			1nm/16μs	
Linewidth CD			7.3±1.3nm	
Line edge roughness (LER)			2.95±0.06nm	
Proximity Effect			Nil	No correction needed

Annexe II: Ion impact Data and Gallium FIB Experiments

Ion track visualization and calculated range data for ions and substrates used in nanolithography (all at 30keV beam energy; 4000 ions).

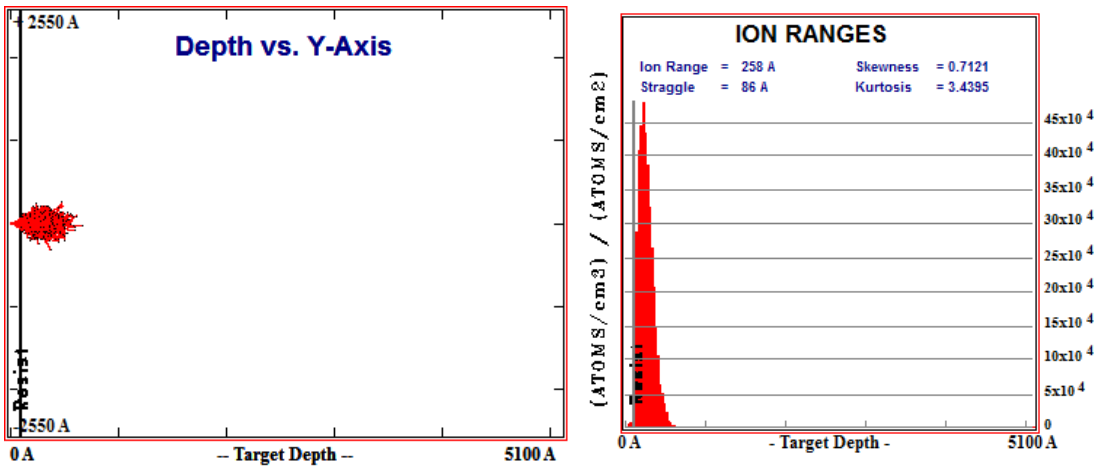

(a) (b)

Fig AII.1 Ga^+ into 10nm thick resist on Si (a) ion tracks (b) Implantation range data

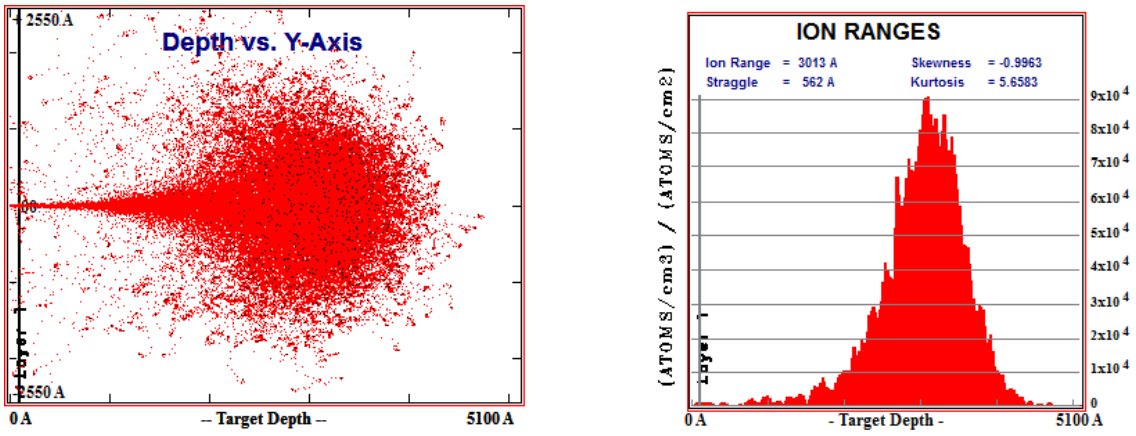

(a) (b)

Fig AII.2 H^+ into 10nm thick resist on Si (a) ion tracks (b) Implantation range data

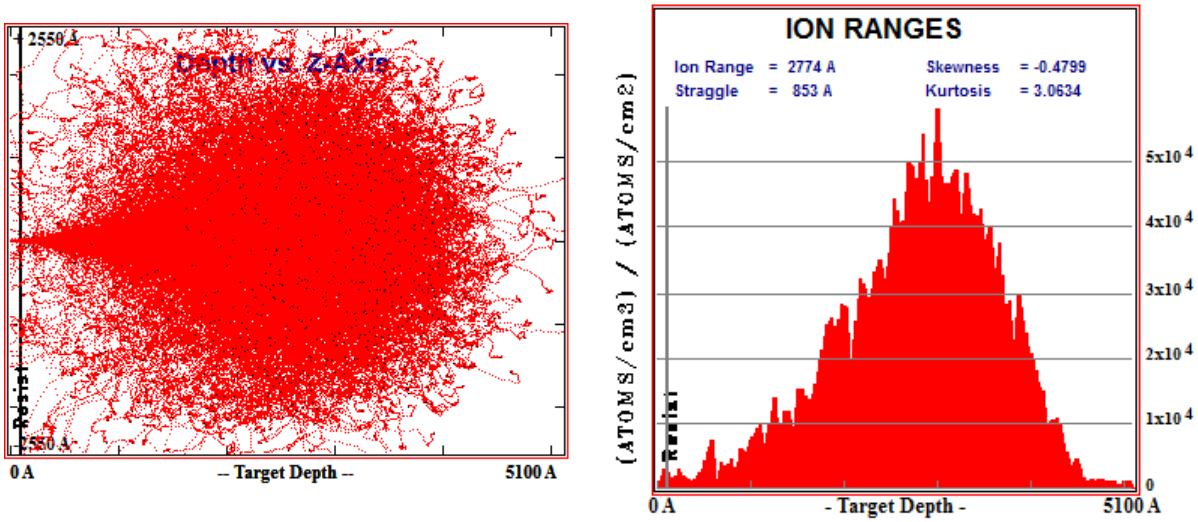

(a) (b)

Fig AII.3 He^+ into 10nm thick resist on Si (a) ion tracks (b) Implantation range data

Ion	Range (nm)	Straggle (nm)
H^+	301	56
He^+	277	85
Ga^+	26	9

Table AII.1 Comparison of implantation range data for singly charged ions used in lithography (10nm thick resist on Si substrate). The straggle is the standard deviation.

The depth distribution of ions for which sputtering can be neglected like He^+ may be approximated analytically to a simple Gaussian with peak value proportional to the ion dose Dcm^{-2}. R is the range and σ is the straggle or standard deviation

$$n(x) = \frac{D}{\sigma\sqrt{2\pi}} e^{-\frac{(x-R)^2}{2\sigma^2}} \qquad \text{AII.1}$$

When sputtering cannot be ignored as in the case of Ga^+ ion impact, the implanted Gaussian profile shifts continuously as the surface of the target is eroded and the implant profile is a sum of Gaussians, i.e. the error function

$$\frac{n(x)}{(\rho/\gamma M)} = \frac{erf\,\frac{R-x}{\sigma\sqrt{2}} + erf\,\frac{x+X-R}{\sigma\sqrt{2}}}{1+erf\,\frac{R}{\sigma\sqrt{2}}} \qquad \text{AII.2}$$

Where ρ, γ are the density and sputter coefficient of the eroded layer and X is the depth of erosion [24]. In this case the implant profile has a peak at the surface of the target $x = 0$ instead of at the range depth $x = R$. An additional important difference is that He^+ ions are electronically inert in the semiconductor signal, whereas Ga^+ are a p-type dopant, albeit one with a low solid solubility [25]. Thus, while large doses of He^+ tend to cluster into bubbles beneath the substrate surface, large Ga^+ doses tend to form liquid Gallium precipitates at the surface.

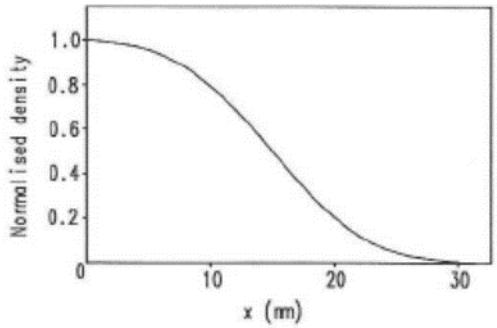

Fig AII.3 Implanted ion distribution for Ga^+ showing effect of sputter erosion [24]

The effects of the Ga^+ implantation becomes apparent in a number of applications such as the fabrication of Si nanowires. In this process, Ga^+ implant lithography is used to write patterns of contact pads and nanowires [26] (investigated in the framework of SNM). This produces a nascent 2D image of the structure which was etched out to form the system of contact pads and suspended nanowires using a plasma etchant of SF_6 and O_2 gases in the STS100 DRIE system at Birmingham University. The resulting nanowires are seen in the SEM image of Fig AII.4 in which the suspended NWs terminate in sheet terminals of Ga implanted Si. The undercut support pillars are visible through the contact sheets due to electron penetration in the SEM,

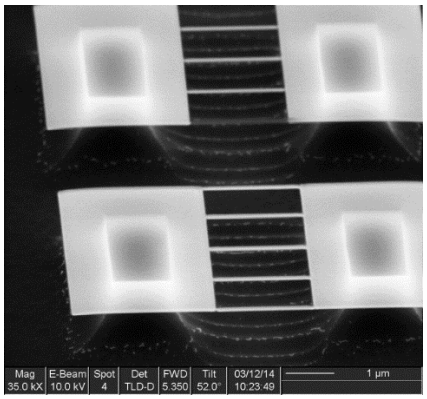

Fig AII.4 SEM image showing suspended Si nanowires 100nm x 2µm formed using Ga^+ implantation etch stop with SF_6/O_2 plasma etch. Ion implant dose 10^{17} ions/cm^2

The low solid solubility of the gallium in silicon systems means that the implanted Ga can form liquid precipitates as shown in Fig AII.5 for a 40nm NW where nanodroplets of gallium are visible post etching. Regular spacing of the nanodroplets or beads along the NWs are consistent with hydrodynamic theory of NWs [27].

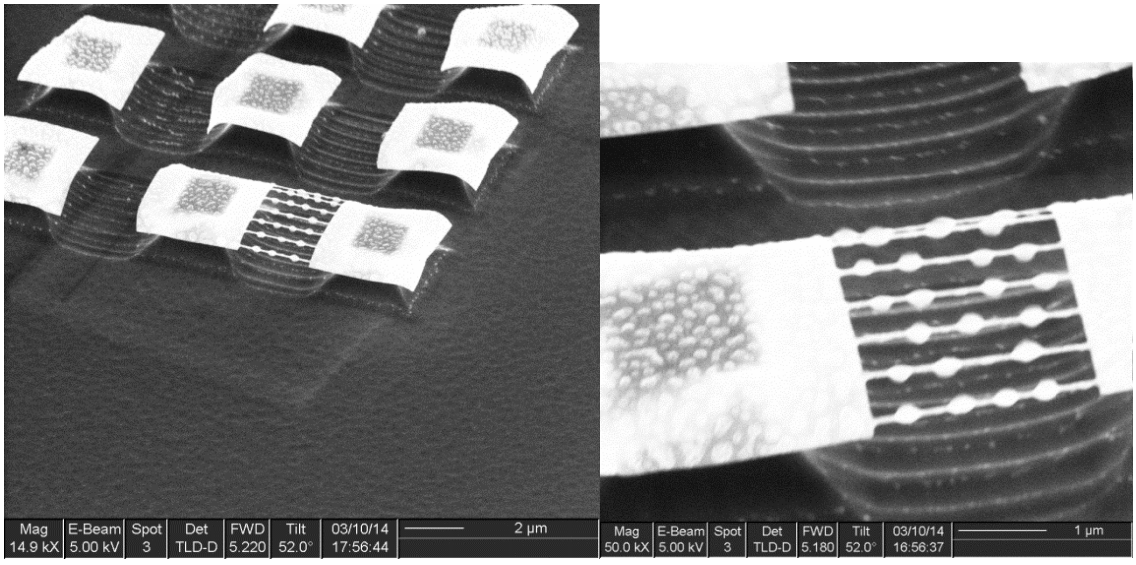

Fig AII.5 Effect of excess dose of Ga^+: surface saturation of Gallium forms droplet precipitates during plasma etch. Ion dose (40nm width) $3x10^{16}$ cm^{-2}

As the yield stress for Ga is much smaller compared to Si, the formation of these instabilities is mainly due to the implanted Ga ions. The critical diameter for the Gallium is about 35nm [28], which is close to the 40nm diameter of the fabricated nanowire. The wavelength is $\lambda_m \approx \sqrt{2}(2\pi R)$ which gives the value of approximately 184nm. The SEM measurements in

Fig AII.5 clearly show ordering of the liquid gallium beads along the NWs with a periodicity of 200nm which is close to the expected value of the wavelength of liquid standing waves from Rayleigh-Plateau theory [27, 28]. These results are consistent with other reported studies for liquid in fibre systems [29]; further details are contained in Aydin Sabouri's PhD thesis [26].

The surface segregation of implanted Ga atoms which is responsible for these phenomena are mirrored in the case of He^+ implantation, though in that case because of the absence of any significant sputter erosion, the implanted helium has a Gaussian distribution centred at a range of ~300nm into the target rather than the error function distribution of Ga. The He atoms accumulate beneath the surface and form bubbles, the pressure from which distorts the surface of the silicon through the formation of bumps, as shown in Fig AIII.6. This phenomenon is more likely to occur in He^+ microscopy than in SHIBL because of the higher doses required to achieve good image statistics. This topic is discussed more fully in SNM report D7.6 (A Kis et al).

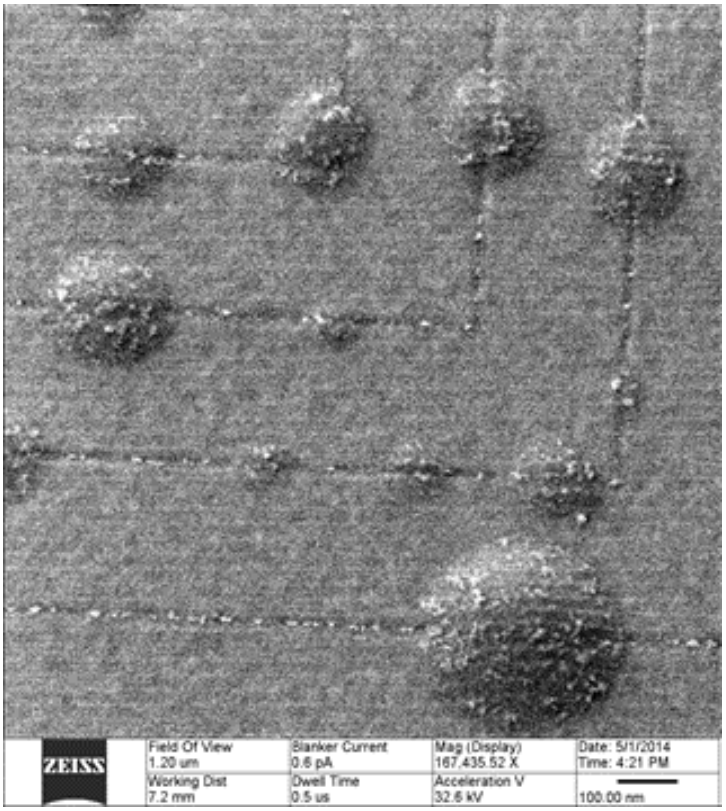

Fig AII.6 HIM image of eSPL patterned calixarene showing surface bumps with Au nanocluster decoration. The bumps are due to accumulated pockets of He gas due to ion implantation during image capture.

Annexe III: Novel Fullerene Resists for SHIBL: Solvent Effects

The following paper which describes the formulation and application of resists for SHIBL developed and optimized in collaboration has been submitted for publication in the Elsevier journal Microelectronic Engineering.

Solvent Effects in a Fullerene Resist for Scanning Helium Ion Beam Lithography

X Shi[1], D X Yang[2,3], S E Huq[4], S A Boden[1], D M Bagnall,[5]

T A Lada II[6], A P G Robinson*[3] and P D Prewett[4]

[1] Electronics and Computer Science, University of Southampton, Southampton SO17 1BJ, UK

[2] Nanoscale Physics Research Laboratory, School of Physics and Astronomy, University of Birmingham, Birmingham, B15 2TT, UK

[3] School of Chemical Engineering, University of Birmingham, Birmingham, B152TT, UK

[4] Oxford Scientific Consultants Ltd., 67 High Street, Dorchester on Thames, Oxfordshire OX10 7HN, UK

[5] Faculty of Engineering, The University of New South Wales, Sydney NSW 2052, Australia

[6] Nano-C Inc., 33 Southwest Park, Westwood, MA 02090, USA

* Corresponding Author: a.p.g.robinson@bham.ac.uk

Keywords: Scanning Helium Ion Beam Lithography, Fullerene Resist

Abstract

In pursuit of a high resolution negative tone resist for use in scanning helium ion beam lithography, a soluble derivative of the C_{60} fullerene molecule is used. This provides an excellent combination of nanoscale patterning capability with low line edge roughness and high durability in plasma etch. The formulation is soluble in a range of solvents and can be spin coated to thicknesses down to 10nm. The effects of casting solvent choice are evaluated. Linewidths of 8nm with low LER have been achieved.

1 Introduction

Helium ion lithography dates back nearly 30 years,[1] but until recently had limited utility due to poor resolution compared to the more common electron beam lithography (EBL) technique. However, the recent realisation of extremely bright and highly stable gas field ion sources, and of improved ion optics, has enabled sub nanometer helium ion beam diameters,[2] which have significantly improved the lithographic performance.[3] With such a tightly focussed beam the primary advantages of helium ions over electrons become apparent.

A 30 keV helium ion beam will deposit energy into materials via the generation of secondary electrons with a typical energy of ~2 eV and will generate virtually no secondaries with energies greater than 20 eV. A 30 keV electron beam on the other hand will generate secondaries with an average energy of 5–15 eV and some with energies in excess of 100 eV.[4] The long range of such high-energy secondary electrons contributes to the proximity effect which limits the resolution of electron beam lithography, in particular for dense patterns. In addition to a significantly reduced proximity effect, scanning helium ion beam lithography (SHIBL) benefits from less beam spreading in the resist (sometimes referred to as secondary electron blur), which limits ultimate resolution in EBL, even for isolated features. The lower penetration depth of helium ions into the resist also leads to improved sensitivity over EBL. Scanning Helium Ion Beam Lithography therefore shows promise for prototyping and fabrication of "beyond CMOS" devices [5] which are defined by innovative new architecture, operating principles, heterogeneous materials, and—most importantly for

lithography—scaling to sub–10 nm feature sizes.[6] One final but vitally important key to the success of this technique is the development of a high resolution and high sensitivity helium ion beam resist, with appropriate etch transfer capabilities and reproducibility, so as to fully realise SHIBL's potential for the single nanometre beyond CMOS regime.

Hydrogen silsesquioxane (HSQ) is a popular high-resolution inorganic negative tone resist for electron beam lithography capable of resolving dense line-space patterns at a pitch of 9 nm [7] in EBL with excellent etch transfer capability.[8] Using SHIBL, line-space patterns on a pitch of 20 nm were written with a line dose of 232 pC/cm, in a 25 nm film of HSQ and developed using a saline solution (1% NaOH and 4% NaCl in deionized water) [5] while 10 nm pitch line-space patterns patterned at 110 pC/cm line dose have been resolved in a 12 nm thick film of the same resist using saline development [9] and 6 nm dots on a 14 nm pitch have been written in a 5 nm thick film of HSQ using M351 alkaline developer.[10] The areal sensitivity of the resist was found to be ~31 μC/cm^2 in SHIBL—more than four times faster than for EBL. However, concerns remain about reproducibility in HSQ. It is well known, for example, that achievable feature size in HSQ is a function of the time between exposure and development, which is highly disadvantageous in direct write lithography processes such as EBL and SHIBL.[11] The effects of delay are exacerbated in a complex manner by patterning conditions, humidity, film thickness, underlayer choice and other factors, making HSQ unsuitable for complex patterning tasks.

Poly(methylmethacrylate) (PMMA) is a widely used high-resolution organic resist for electron beam lithography. Feature sizes of 20 nm can routinely be achieved and, utilising cold development, 10 nm lines on a 30 nm pitch have been patterned using 1.2 nC/cm line dose.[12] Megasonically assisted development has been used to achieve isolated lines with linewidths of 2–3 nm.[13] Dense line-space patterns have been produced in PMMA with a pitch of 40 nm, and dense dot arrays with a pitch of 25 nm have been achieved using pure isopropyl alcohol (IPA) development.[14] Using SHIBL lines with a width of 14.5 nm on a 100 nm pitch have been achieved in 20 nm thick PMMA films in both positive and negative tone modes.[15] A dose of 250 μC/cm^2 was used for positive tone patterning whilst 2.5 mC/cm^2 was required to pattern in the negative tone. It

can be seen that the resolution of PMMA in SHIBL does not yet match its performance in EBL. More problematically, PMMA also suffers from very low etch durability, making subsequent pattern transfer difficult.[16]

It therefore remains the case that an optimal resist for helium ion beam lithography is an essential requirement. Such a resist should demonstrate stability during and after patterning, and reproducible behaviour with wide environmental tolerance, together with high-resolution capability, high sensitivity, good etch durability, and standard processing requirements, such as deposition via spin-coating. The ideal resist will face a significant number of difficult challenges, as detailed below.

Due to unbalanced capillary forces during the drying stage of typical photoresist wet development, the maximum aspect ratio (resist film thickness/feature width) is limited. If the aspect ratio exceeds a value known as the critical aspect ratio of collapse (CARC), then extensive pattern collapse will occur in the resist. Conventionally, a thickness/feature-width ratio of between 3:1 and 4:1 is achievable. However, this is known to decrease, due to increased capillary forces, as the pitch is reduced, [17] falling below 2:1 at pitches of 60 nm.[18] Furthermore, as the required resist film thickness decreases below 100 nm, interfacial effects become dominant in the film and its modulus decreases drastically from the bulk value,[19] which has led to a further increase in the rate of reduction in the CARC towards 1:1.[20] This has forced the adoption of resist films with sub 20-nm thicknesses to address the highest resolutions.

At the same time line edge roughness (LER), defined as the deviation of a real feature from the idealised shape, and which strongly affects device performance, becomes increasing detrimental at small feature sizes. LER will tend to increase as the pitch decreases due to material stochastics (eg formulation variation), imaging stochastics (eg shot noise) [21] and aerial image quality.[22] It has also been shown that, as film thickness is reduced, the LER will tend to increase. This is due both to a reduction in the averaging effect of the film thickness on sidewall roughness and an increase in the importance of the resist-substrate interface area (resist footing),[23] but also due to material stochastics in the film.[24] Therefore, whilst it is necessary to reduce film thickness to avoid pattern collapse and enable ultra-high resolution patterning, it is essential also to be mindful of line edge

roughness failure modes. Simulations indicate that so-called molecular resist films (utilising small molecule materials rather than polymeric components) are more resistant to line edge roughness effects.[24,25]

Finally, once a pattern has been created and developed it must be transferred to the substrate to create a device. Often the resist pattern will be transferred using plasma etching either directly in to the substrate, or into a hardmask stack to create a suitable mask for subsequent metallization or doping.

Whilst the use of a molecular resist may therefore allow for the use of thin films to avoid pattern collapse, simultaneously supressing detrimental line edge roughness, the task of pattern transfer from such thin materials into semiconductor substrates using traditional plasma etching techniques remains challenging. In order to enable such etch transfer it is necessary to provide a resist with an exceptionally high etch durability under typical etchant process gases. One of two empirical models are typically used to predict the etch durability of photoresist materials. The Ohnishi number (ON) [27] is given by equation 1:

$$ON = \frac{N}{N_C - N_O} \quad (1)$$

where N is the total number of atoms in a resist molecule, N_C the number of carbon atoms, and N_O the number of oxygen atoms. In this model a low number indicates a high etch durability. Increasing the proportion of carbon and decreasing the proportion of oxygen will therefore improve the etch durability of the resist. Typically, resist polymers range from a value of 2–3 for the most durable, such as novolac or polyhydroxystyrene (PHS) based resists, to 6–8 for the least durable such as PMMA. The second model, known as the ring parameter (RP),[28] addresses the experimental observation that aromatic polymers are typically more etch resistant, and is given by equation 2:

$$RP = \frac{M_{ring}}{M_{tot}} \quad (2)$$

where M_{ring} is the mass of carbon in ring structures, and M_{tot} is the total mass of the resist molecule. In this case a higher value indicates better etch durability, and is achieved by increasing the number of carbon ring structures in the resist. PMMA has an *RP* of 0, compared with 0.6 for PHS. A number of more complicated models, reviewed in [29] can be used to examine the details of particular molecular structures, but the Ohnishi and Ring models are sufficient to guide general resist design for high etch durability.

All of these factors must therefore be taken in to account in resist design. In order to enable sub-10 nm patterning, an ultra-thin resist film, with small molecular units is indicated. Enabling pattern-transfer via plasma etching leads to a requirement for the highest possible carbon content in the resist, with as many of the carbons in a ring structure as possible. The material chosen to meet these requirements was therefore based on a monoadduct methanofullerene derivative. It is self-apparent that the nature of the fullerene molecule itself, with its 60 carbon atoms in a three dimensional cage or ring structure, gives the maximum possible ring parameter value and the minimum possible Ohnishi number. Additionally fullerene is a small molecule (<1 nm diameter) that forms amorphous films, and that has been shown to be suitable for electron beam lithography.[30] However, fullerene is not easily spin coated due to the very low solubility in all solvents. This can be addressed through the derivatisation of the fullerene molecule to enhance the solubility in appropriate spin coating solvents. A large number of fullerene derivatives have been spin coated and patterned using electron beam lithography for instance as shown in [31] and [32]. For the development of an ultra-thin film, ultra-high resolution resist for He ion beam, an easily synthesised fullerene derivative with high overall carbon content and good solubility in appropriate spin coating solvents was identified and used as the basis of the proprietary resist IM-HM-01 (Irresistible Materials Ltd). The structural class of the fullerene derivative is indicated in figure 1.

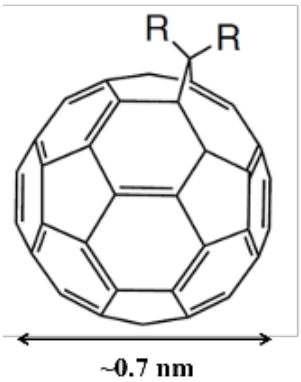

Figure 1: Schematic of a mono-adduct methanofullerene derivative.

Previously we have described the SHIBL patterning of dense features in this resist. Line-space patterns with a pitch of down to 12 nm were demonstrated at a line dose of 40 pC/cm in a resist film of 10 nm thickness.[33] Here we present the effects of the spin-coating solvent choice on the SHIBL patterning of isolated lines in the IM-HM-01 resist.

2 Experimental

To synthesise the material fullerene was added to a flask of degassed o-dichlorobenzene at a concentration of 20 g/L. To the solution was added 1 mol eq. of precursor and 1 mol eq. of an organic base. The solution was heated to 80 °C under argon and stirred while exposed to visible light. The reaction progress was monitored by HPLC, and when complete, the heat and light turned off. Upon reaching room temperature, the solution was filtered. The filtrate was purified by chromatography over silica gel using o-dichlorobenzene and toluene. The unreacted fullerene was collected first, followed by the desired product, which was subjected to rotary evaporation until concentrated, then precipitated by the addition of an excess of methanol. The mixture was filtered, and the product was dried under vacuum at 50 °C overnight. The resultant medium-brown powder was checked for dryness by TGA (<2% residual solvent) and purity by HPLC (>99.5%). The carbon content of the material was found to be ~95 wt%; the Ohnishi parameter was ~1.26, and the ring parameter ~0.87.

The resist can be formulated in various solvents, including chloroform, chlorobenzene or

anisole. Chloroform was rejected as a solvent for SHIBL patterns due to poor results seen in EBL patterning and due to its hazardous nature. Chlorobenzene and anisole are the typical solvents utilised for PMMA resist formulations, and were adopted for this study. The resist was formulated at 5 g/l in each solvent and filtered with a 200 nm teflon syringe filter prior to spin coating.

For these experiments samples were produced on 20 × 20 mm chips, which were diced from a 100 mm wafer (Si-Mat, n-type, <100>). After dicing, the chips were cleaned using semiconductor grade chemicals. Chips were washed ultrasonically in IPA for 15 minutes and then 1 minute in flowing deionised (DI) water (Purite Neptune, 18.2 MΩcm). A hydrogen terminated surface was prepared on the chips using a 10 minute dip in H_2SO_4 (95 – 98%) / H_2O_2 [1:1], followed by a 1 minute dip in flowing DI, a 1 minute dip in a weak aqueous solution of hydrofluoric acid, and finally a further 1 minute rinse in flowing DI water. The substrates were then dried with nitrogen and used immediately. For fresh undiced wafers the cleaning step was not required. HMDS primer treatment of the silicon is contra-indicated.

For small samples a resist dispense of 50 to 100 µl per chip was used, whilst 1 – 2 ml was dispensed for 100 mm wafer coating. No spreading step was utilised and the spin coater was set to ramp to full speed with maximum acceleration. Chips were spun for 60 s, before receiving a post exposure bake of 70 °C for 5 min. The film thickness was measured using a surface profiler (Dektak 3st Auto).

An Orion Plus Helium Ion Microscope (HIM, Carl Zeiss) with Xenos pattern generator and beam blanker unit was used for helium ion exposures. A beam voltage of 30 kV was used in all cases. For large area exposures the beam current was set to 5 pA, whilst high resolution patterning was undertaken using a current of 0.5 pA. Electron beam exposures were undertaken using a Gemini FEG-SEM (NVision 40 FIB SEM) with a beam voltage of 30 kV and a beam current of 5.8 nA for large area exposures, and an XL30 SFEG (FEI) with Raith pattern generator, at a beam voltage of 30 kV and current of 0.5 nA for high resolution patterns. Resist sensitivity was evaluated by patterning an array of 5 µm × 10 µm areas with doses ranging from 0–288 µC/cm^2 (SHIBL) or 0–205 mC/cm^2 (EBL), and the residual film thickness measured with AFM as detailed elsewhere.[33] Samples were developed

in cyclohexanone for 20 s then rinsed in IPA before being dried with nitrogen, unless otherwise specified. No post exposure bake was applied prior to development. High-resolution SHIBL samples were imaged using the HIM, whilst the high-resolution EBL patterns were imaged with the XL30 SFEG.

3 Results

Films of the resist were coated on to silicon chips by spin coating. The resist formulation concentration was held constant whilst the spin speed was varied. Figure 2(a) shows the results for IM-HM-01 formulated in anisole (IM-HM-01A). Smooth films were observed for all spin speeds up to 7000 rpm. Figure 2(b) shows the results for IM-HM-01 formulated in chlorobenzene (IM-HM-01C).

Figure 2: Thickness versus spin speed using (a) anisole, and (b) chlorobenzene casting solvents

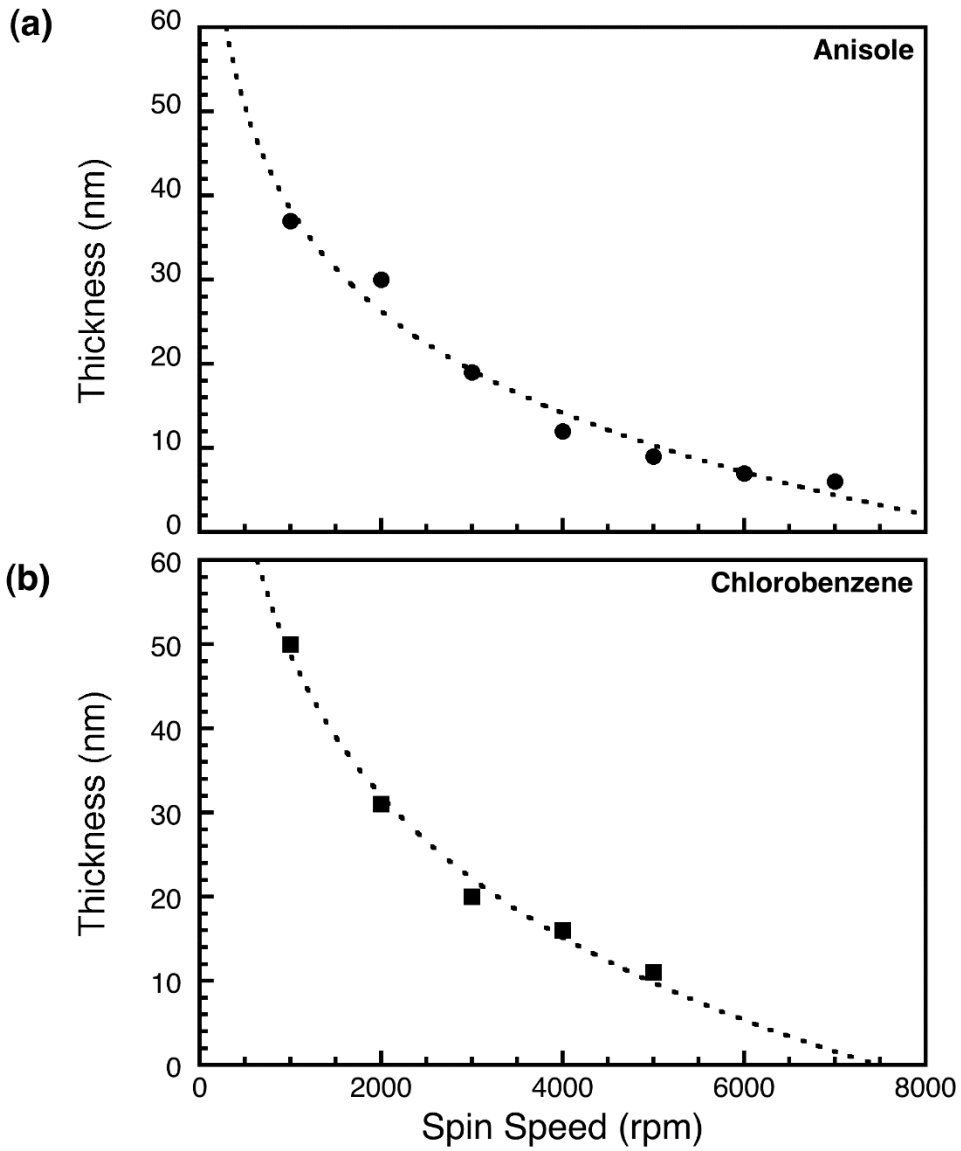

In this case smooth films were seen for spin speeds up to 5000 rpm. Films were apparent in the range 6000–8000 rpm but were insufficiently smooth to make an accurate thickness measurement. Films spun from anisole were on average ~15% thinner than those spun from chlorobenzene. Thicker films up to 120 nm have been prepared at higher formulation concentrations.

The response of the resists to helium ion, and to electron irradiation was evaluated at 30 kV in both cases, with cyclohexanone development. Figure 3 shows the responses of IM-HM-01A and IH-HM-01C after exposure to a range of doses of helium ions. The sensitivity, taken for a negative tone resist as the dose at which 50% of the film is retained after development, is 30 μC/cm^2 for the chlorobenzene solvent and 50 μC/cm^2 for the anisole solvent. The contrast for

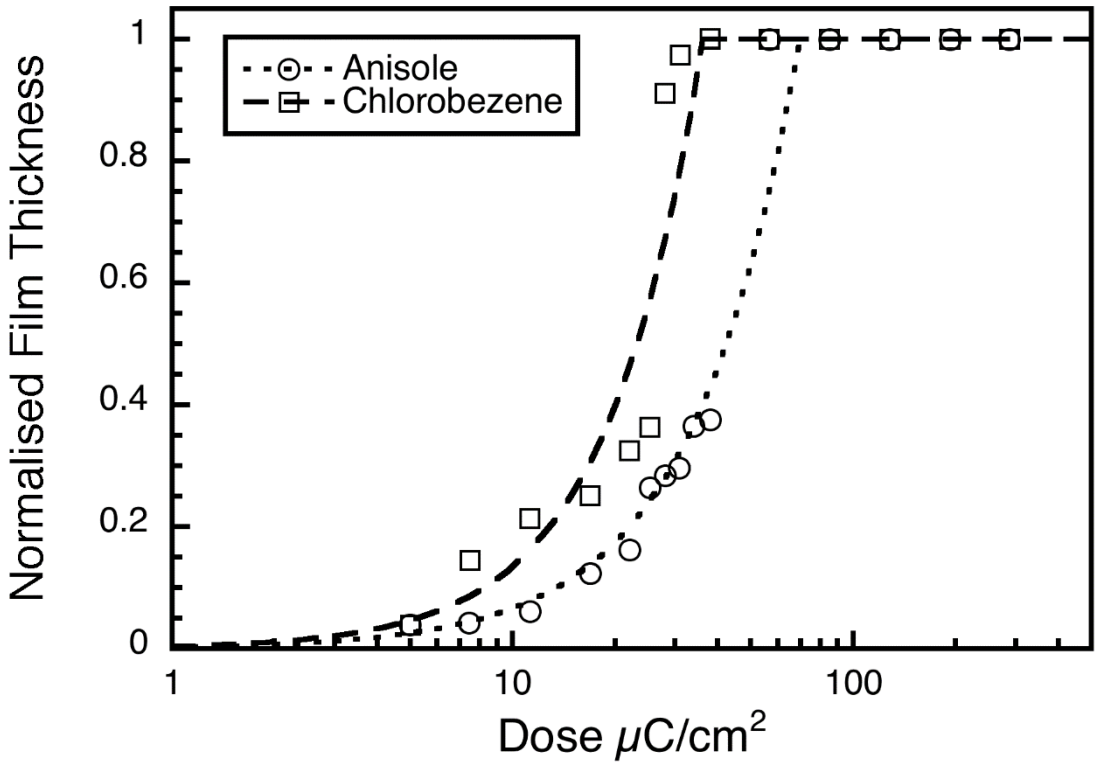

Figure 3: Helium ion beam dose response curve for IM-HM-01A and IM-HM-01C.

both formulations was approximately 3. The electron beam response is shown for comparison in

figure 4. A significantly higher dose of ~20 mC/cm² is required for 50% retention of the film in this case. This indicates that the resist is between 400 and 667 times faster when exposed with helium ions, depending on the solvent used, when compared with e-beam exposure.

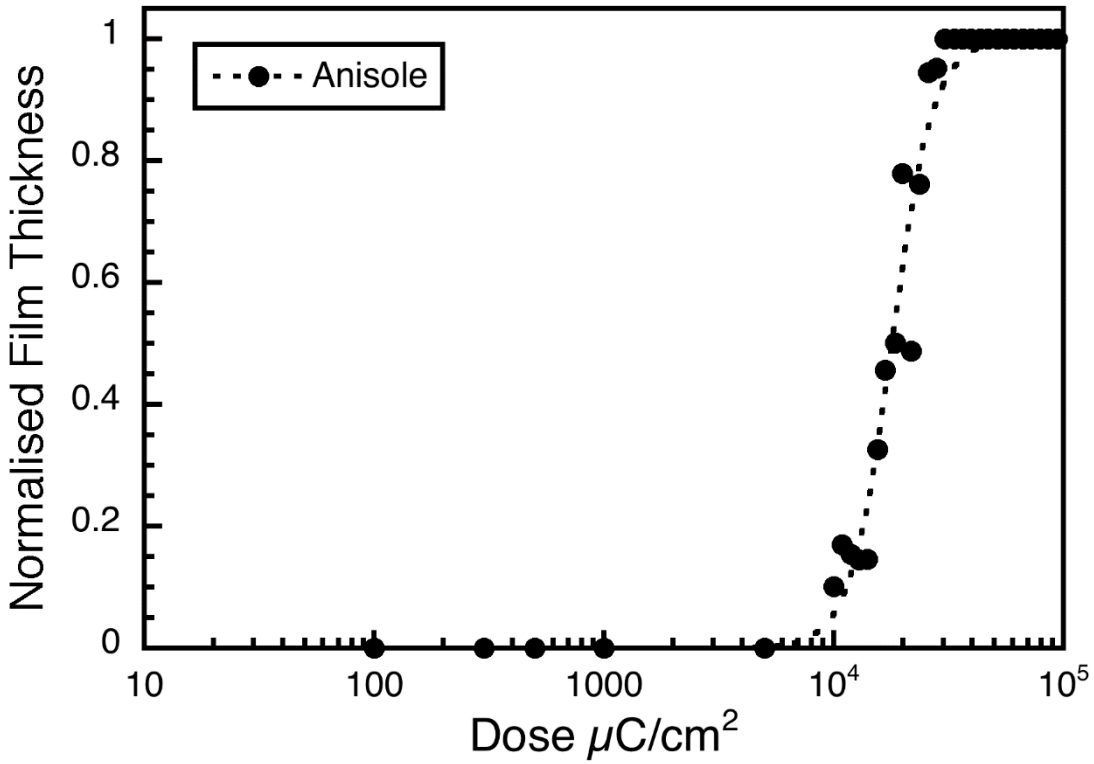

Figure 4: Electron beam dose response curve for IM-HM-01A.

Using the XL30 SFEG the minimum achievable EBL pitch for single pixel lines at 30 kV was evaluated with two casting solvents and two developers. Figures 5(a) and (b) show films that were spin coated from a chloroform solution, and developed in chlorobenzene:IPA [1:1] and cyclohexanone respectively. Figure 5(c) was spin coated from an anisole solution and developed in cyclohexanone. For chloroform casting solvent and chlorobenzene:IPA developer (Figure 5(a)) ~16 nm linewidths on a pitch of 36 nm were achieved

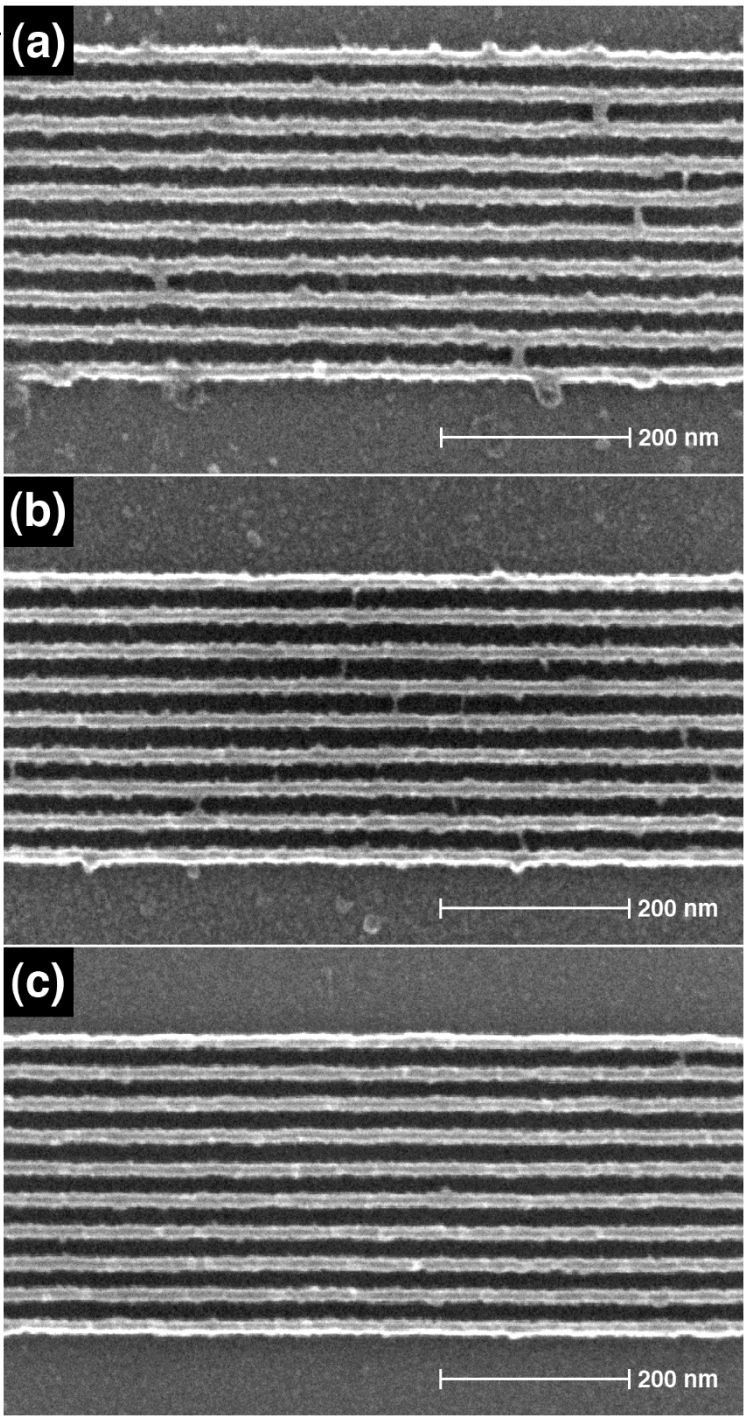

Figure 5: Electron beam patterned single pixel lines in (a) IM-HM-01 resist cast from chloroform and developed in a [1:1] mixture of chlorobenzene and IPA. The pitch is 36 nm and a line dose of 78 nC/cm was used; (b) IM-HM-01 resist cast from chloroform and developed in cyclohexanone. The pitch is 32 nm and a line dose of 115 nC/cm was used; (c) IM-HM-01 resist cast from anisole and developed in cyclohexanone. The pitch is 32 nm and a line dose of 104 nC/cm was used.

using a line dose of 78 nC/cm. The lines demonstrate a high degree of line edge roughness and

bridging. Changing to the cyclohexanone developer improved the quality of the lines (Figure 5(b)) and enabled linewidths down to ~14 nm to be achieved at 32 nm pitch with a line dose of 115 nC/cm, whilst the smoothest lines were seen with the anisole casting solvent and cyclohexanone development (Figure 5(c)). Linewidths of ~13 nm were written on a pitch of 32 nm at a line dose of 104 nC/cm.

Finally the lithographic performance of the resist with SHIBL was evaluated for isolated line arrays using both chlorobenzene and anisole casting solvents. Arrays of single pixel lines, with length 1.5 μm and pitch 100 nm where patterned in 10 nm thick films of IM-HM-01C and IM-HM-01A on silicon as shown in Figures 6(a) and (b) respectively. The line dose was varied from 10 pC/cm to 510 pC/cm in 18 steps. The optimum dose, judged as the lowest dose

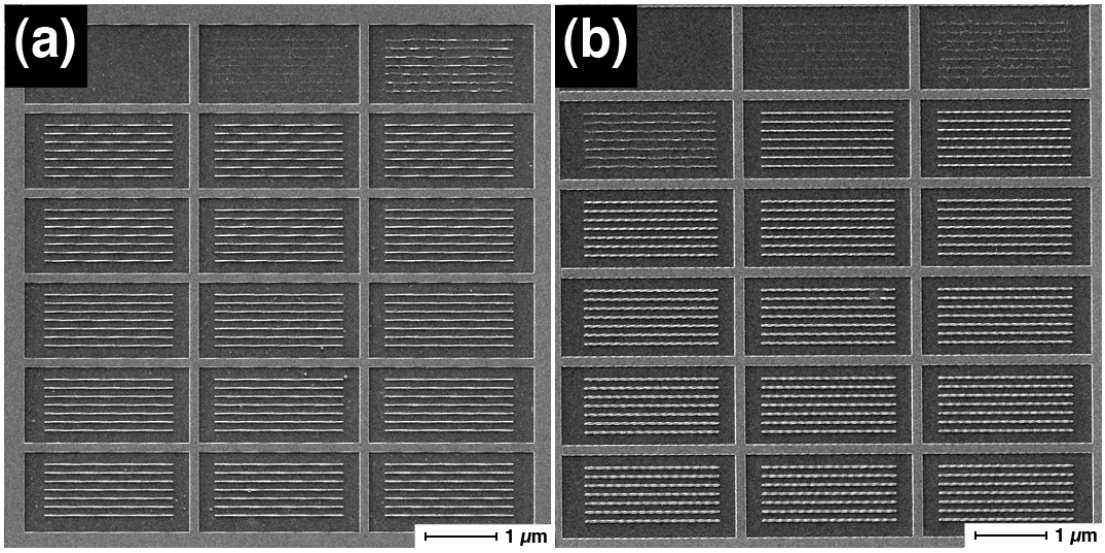

Figure 6: Arrays of isolated single pixel lines patterned by SHIBL on a pitch of 100 nm at a range of doses in (a) IM-HM-01C, and (b) IM-HM-01A resists.

for which continuous lines were patterned, was found to be 130 pC/cm for IM-HM-01C, whilst for IM-HM-01A a dose 100 pC/cm was required. Figures 7(a) and (b) show the ultimate resolution for the resist under these conditions. IM-HM-01C was capable of patterning with an isolated line resolution of 12 nm, while IM-HM-01A performed significantly better, achieving a minimum linewidth of 8 nm. Some indications that further reductions in linewidth may be possible have been reported elsewhere.[33]

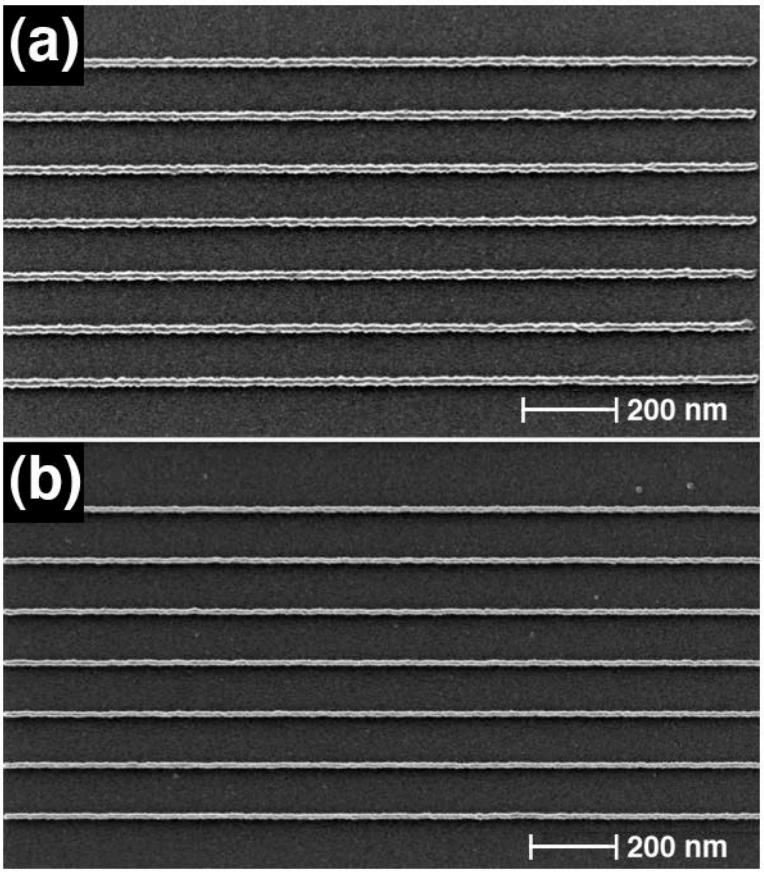

Figure 7: Isolated single pixel lines patterned by SHIBL on a pitch of 100 nm (a) IM-HM-01C at a line dose of 130 pC/cm giving a linewidth of 12 nm, and (b) IM-HM-01A at a line dose of 100 pC/cm giving a linewidth of 8 nm.

4 Conclusions

A soluble derivative of the C_{60} fullerene molecule has been used to formulate a high resolution, high sensitivity resist for use in scanning helium ion beam lithography (SHIBL) This provides an excellent combination of nanoscale patterning capability with low line edge roughness and extraordinarily high durability in plasma etch, as presented elsewhere.[34] Fullerene resists do not suffer from post exposure delay line broadening and are thus suitable for serial patterning processes such as EBL and

SHIBL. The performance of the resist in two casting solvents – chlorobenzene and anisole is compared. The former improves sensitivity slightly but with a significant impact on the achievable resolution in isolated features. In anisole solvent, the resist IM-HM-01A can be reproducibly coated to sub-10 nm film thicknesses, and patterned with sub-10 nm features. Linewidths of 8nm with low LER have been achieved.

Acknowledgements

The research leading to these results has received funding from the European Union Seventh Framework Programme FP7/2007–2013 under grant agreement No. 318804 (SNM). The authors would like to thank the Engineering and Physical Sciences Research Council (EPSRC) for support of this project. The authors thank Irresistible Materials Ltd. for support and provision of resist materials. The Disco DAD 321 wafer dicer used in this research was obtained through the Birmingham Science City provided: Creating and Characterizing Next Generation Advanced Materials, with support from Advantage West Midlands (AWM) and part funded by the European Regional Development Fund (ERDF). D.X.Y. thanks The University of Birmingham and China Scholarship Council (CSC) for support. D.X.Y and A.P.G.R. gratefully acknowledge the support and assistance of Professor R E Palmer.

References

[1] Horiuchi K, Itakura T, Ishikawa H. Fine pattern lithography using a helium field ion source. *J Vac Sci Technol B* 1988;**6**:241–4.

[2] Morgan J, Notte J, Hill R, Ward B. An introduction to the helium ion microscope. *Microsc Today*

2006;**14**:24–31.

[3] Ocola LE, Rue C, Maas D. High-resolution direct-write patterning using focused ion beams. *MRS Bull* 2014;**39**:336–41.

[4] Shi X and Boden SA. Scanning helium ion beam lithography *in* Materials and Processes for Next Generation Lithography. Robinson APG and Lawson RA, eds. 563–94. Oxford, UK: Elsevier; 2016.

[5] Sidorkin V, van Veldhoven E, van der Drift E, Alkemade P, Salemink H, Maas D. Sub-10-nm nanolithography with a scanning helium beam. *J Vac Sci Technol B,* 2009;**27**:L18–20.

[6] The international technology roadmap for semiconductors. 2015 ed. 2015. http://www.itrs2.net/itrs-reports.html.

[7] Yang JK, Cord B, Duan H, Berggren KK, Klingfus J, Nam SW, Kim KB, Rooks MJ. Understanding of hydrogen silsesquioxane electron resist for sub-5-nm-half-pitch lithography. *J Vac Sci Technol B* 2009;**27**:2622–7.

[8] Welch CC, Goodyear AL, Wahlbrink T, Lemme MC, Mollenhauer T. Silicon etch process options for micro- and nanotechnology using inductively coupled plasmas. *Microelectron Eng* 2006;**83**:1170–3

[9] Li WD, Wu W, Williams RS. Combined helium ion beam and nanoimprint lithography attains 4 nm half-pitch dense patterns. *J Vac Sci Technol B* 2012;**30**:06F304.

[10] Winston D, Cord BM, Ming B, Bell DC, DiNatale WF, Stern LA, Vladar AE, Postek MT, Mondol MK, Yang JKW, Berggren KK. Scanning-helium-ion-beam lithography with hydrogen silsesquioxane resist. *J Vac Sci Technol B* 2009;**27**:2702–6.

[11] Olynick D, Schwartzberg A, Keszler DA. Mainstreaming inorganic metal-oxide resists for high-resolution lithography *in* Materials and Processes for Next Generation Lithography. Robinson APG and Lawson RA, eds. 349–75. Oxford, UK: Elsevier; 2016.

[12] Hu W, Sarveswaran K, Lieberman M, Bernstein GH. Sub-10 nm electron beam lithography using

cold development of poly(methylmethacrylate). *J Vac Sci Technol B*2004;**22**:1711–6

[13] Küpper D, Küpper D, Wahlbrink T, Bolten J, Lemme MC, Georgiev YM, Kurz H. Megasonic-assisted development of nanostructures. *J Vac Sci Technol B* 2006;**24**:1827–32.

[14] Dial O, Cheng CC, Scherer A. Fabrication of high-density nanostructures by electron beam lithography. *J Vac Sci Technol B* 1998;**16**:3887–90.

[15] Sidorkin VA. Resist and exposure processes for sub-10-nm electron and ion beam lithography [Ph.D. thesis]. Delft University of Technology; 2010.

[16] Gogolides E, Argitis P, Couladouros EA, Vidali VP, Vasilopoulou M, Cordoyiannis G, Diakoumakos CD, Tserepi A. Photoresist etch resistance enhancement using novel polycarbocyclic derivatives as additives. *J Vac Sci Technol B* 2003;**21**:141–7.

[17] Hien S, Rich G, Molina G, Cao HB, Nealey PF. Collapse behavior of single layer 193 and 157 nm resists: Use of surfactants in the rinse to realize the sub 130 nm nodes. *Proc SPIE* 2002;**4690**:254–261.

[18] Yoshimoto K, Higgins C, Raghunathan A, Hartley JG, Goldfarb DL, Kato H, Petrillo K, Colburn ME, Schefske J, Wood O, Wallow TI. Revisit pattern collapse for 14nm node and beyond. *Proc SPIE* 2011;**7972**:79720K.

[19] Stafford CM, Vogt BD, Harrison C, Julthongpiput D, Huang R. Elastic moduli of ultrathin amorphous polymer films. *Macromolecules*. 2006;**39**:5095–9.

[20] Carcasi M, Bassett D, Printz W, Kawakami S, Miyata Y. Line-pattern collapse mitigation status for EUV at 32nm HP and below. *Proc SPIE* 2012;**8325**:83250K.

[21] Naulleau P. EUV lithography patterning challenges *in* Materials and Processes for Next Generation Lithography. Robinson APG and Lawson RA, eds. 349–75. Oxford, UK: Elsevier; 2016.

[22] Shumway MD, Naulleau P, Goldberg KA, Bokor J. Measuring line roughness through aerial image

contrast variation using coherent extreme ultraviolet spatial filtering techniques. *J Vac Sci Technol B* 2005;**23**:2844–7.

[23] Ekinci Y, Vockenhuber M, Terhalle B, Hojeij M, Wang L, Younkin TR. Evaluation of resist performance with EUV interference lithography for sub-22-nm patterning. *Proc SPIE* 2012;**8322**:83220W.

[24] Cardineau B, Early W, Fujisawa T, Maruyama K, Shimizu M, Sharma S, Petrillo K, Brainard R. LER limitations of resist thin films. *J Photopolym Sci Technol* 2012;**25**:633–40.

[25] Drygiannakis D, Patsis GP, Raptis I, Niakoula D, Vidali V, Couladouros E, Argitis P, Gogolides E. Stochastic simulation studies of molecular resists. *Microelectron Eng* 2007;**84**:1062–5.

[26] Drygiannakis D, Patsis GP, Tsikrikas N, Kokkoris G, Boudouvis A, Raptis I, Gogolides E, Argitis P. Stochastic simulation studies of molecular resists for the 32nm technology node. *Microelectron Eng* 2008;**85**:949–54.

[27] Gokan H, Esho S, Ohnishi Y. Dry etch resistance of organic materials. *J Electrochem Soc* 1983;**130**:143–6.

[28] Kunz RR, Palmateer SC, Forte AR, Allen RD, Wallraff GM, Di Pietro RA, Hofer DC. Limits to etch resistance for 193-nm single-layer resists. *Proc SPIE* 1996;**2724**:365–76.

[29] Oehrlein GS, Phaneuf RJ, Graves DB. Plasma-polymer interactions: A review of progress in understanding polymer resist mask durability during plasma etching for nanoscale fabrication. *J Vac Sci Technol B* 2011;**29**:010801.

[30] Tada T, Kanayama T. Nanolithography using fullerene films as an electron beam resist. *Jpn J Appl Phys* 1996;**35**:L63–65.

[31] Robinson APG, Palmer RE, Tada T, Kanayama T, Shelley EJ, Philp D, Preece JA. Exposure mechanism of fullerene derivative electron beam resists. *Chem Phys Lett* 1999;**312**:469–74.

[32] Robinson APG, Palmer RE, Tada T, Kanayama T, Shelley EJ, Philp D, Preece JA. Systematic Studies of Fullerene Derivative Electron Beam Resists. *Proc Mater Res Soc* 2000;**584**:115–20.

[33] Shi X, Prewett PD, Huq SE, Bagnall DM, Robinson APG, Boden SA. Helium ion beam lithography on fullerene molecular resists for sub-10 nm patterning. *Microelectron Eng* 2016;**155**:74–8.

[34] de Marneffe JF, Cooke M, Goodyear A, St. Braithwaite N, Sutton Y, Bowden M, Altamirano-Sanchez E, Zotovich A, El Otell Z, Chan BT, Knoll A, Rawlings C, Duerig U, Spieser M, Kaestner M, Neuber C, Rangelow I. Advanced Etching for Nanodevices and 2D materials. *Presented at MNE 2016* SNM-1-52016. Accessible from: https://www.researchgate.net/publication/308764935_Advanced_Etching_for_Nano-devices_and_2D_materials. (*IM-HM-01A resist is presented under the name MFHM1 in this work*)